Universidade de Aveiro Departamento de Eletrónica, Telecomunicações e Informática

2016

Ana Filipa Pires Afonso

Reducing Linearity Requirements for In-Body Communication in the Medical Implant Communication Service Band

Ana Filipa Pires Afonso

Reducing Linearity Requirements for In-Body Communication in the Medical Implant Communication Service Band

Masters Thesis project presented to the University of Aveiro to fulfil the necessary requirements for obtaining the Master degree in Electronics and Telecommunications Engineering, realized under the scientific supervision of the Dr.-Ing. Gerhard Bauch, Professor and Director of the Communications Institute of Technical University of Hamburg–Harburg (TUHH) and the Doctor Luís Filipe Mesquita Nero Moreira Alves, Assistant Professor of the Electronics, Telecommunications and Informatics Department of the University of Aveiro.

Tese de Mestrado apresentada à Universidade de Aveiro para cumprimento dos requisitos necessários à obtenção do grau de Mestre em Engenharia Eletrónica e Telecomunicações, realizada sob a orientação científica do Prof. Dr.-Ing. Gerhard Bauch, Professor e Diretor do Instituto de Comunicações da Universidade Técnica de Hamburg–Harburg (TUHH) e do Doutor Luís Filipe Mesquita Nero Moreira Alves, Professor Auxiliar do Departamento de Eletrónica, Telecomunicações e Informática da Universidade de Aveiro.

o júri / the jury

presidente / president

Prof. Dr.-Ing. Gerhard Bauch

Professor e Diretor do Departamento de Telecomunicações da Universidade Técnica de Hamburgo–Harburg

vogais / examiners committee

Priv.-Doz. Dr.-Ing. habil. Rainer Grünheid

Professor Auxiliar do Departamento de Telecomunicações da Universidade Técnica de Hamburgo–Harburg

Prof. Doutor Luís Filipe Mesquita Nero Moreira Alves

Professor Auxiliar do Departamento de Eletrónica, Telecomunicações e Informática da Universidade de Aveiro

Jan-Christoph Brumm

Membro da Equipa Científica do Departamento de Telecomunicações da Universidade Técnica de Hamburgo–Harburg

Contents

List of Figures

List of Tables

Acronyms

AWGN	additive white Gaussian noise
ACI	adjacent channel interference
ALC	automatic level control
AM/AM	amplitude-to-amplitude transfer function
AM/PM	amplitude-to-phase transfer function
ACLR	adjacent channel leakage ratio
BAN	body area network
BSN	body sensor network
BCH	Bose-Chaudhuri-Hocquenghem
bps	bits per second
BPSK	binary phase shift keying
BER	bit error rate
CCA	clear channel assessment
CMOS	complementary metal oxide semiconductor
CPM	continuous phase modulation
CPFSK	continuous phase frequency shift keying
D8PSK	differential 8-phase shift keying
DPSK	differential phase shift keying

EIRP equivalent isotropically radiated power

EVM error vector magnitude

ECE equivalent circuit expression

FCC Federal Communications Commission

FDA Food and Drug Administration

FCS frame check sequence

FDTD finite difference time domain

FSK frequency shift keying

FER Frame error rate

GMSK Gaussian minimum-shift keying

HBC human body communications

HCS header check sequence

IEEE Institute of Electrical and Electronics Engineers

ISM industrial, scientific and medical

IMP intermodulation products

ISI intersymbol interference

IC integrated circuits

LSB least significant bit

LOS line of sight

LREC rectangular frequency pulse length L

LRC	raised cosine, pulse length L
LFSR	linear feedback shift register
MAC	medium access control
MICS	medical implant communication service band
MPDUs	MAC protocol data units
MSK	minimum shift keying
NB	narrowband
NLOS	non-line of sight
NIST	National Institute of Standard and Technology
OSI	open systems interconnection
OQPSK	offset quadrature phase shift keying
PHY	physical-layer
PSDU	physical-layer service data unit
PPDU	physical-layer protocol data unit
PLCP	physical-layer service convergence protocol
PMD	physical medium dependent
PA	power amplifier
PAPR	peak to average power ratio
PSD	power spectral density
PSK	phase shift keying

QAM	quadrature amplitude modulation
RF	radio frequency
RRC	root raised cosine
RC	raised cosine
REC	rectangular frequency pulse
RMS	root mean square
SAR	specific absorption rate
SNR	signal to noise power ratio
SAP	service access point
SSPA	solid state power amplifier
SCS	spinal cord stimulation
UWB	ultra wide-band
WBAN	wireless body area network
WMTS	wireless medical telemetry system
WPAN	wireless personal area network

1 Introduction and Motivation

Today, the average human life expectancy has reached an all time high. The progress in medicine, hygiene and mass vaccination are helping the improvement of life on a daily basis. The medical devices and these factors contribute to a longer and healthier life.

A medical device can be classified as an instrument, an equipment or a material to be use in the human body. These medical devices aim to help with diagnosis, prevention, control and treatment of an illness or injury, study or modification of the anatomy or a physiological process. Which principal intended action is not achieved by pharmacological, chemical, immunological or metabolic methods. On the other hand, the active medical devices implantable operation depends on a source of electricity or a different energy source generated directly by the human body or with gravity. These devices are designed to be fully or partially introduced into the human body through a surgery – with the intention of remain after the operation.

The first steps in bioengineering were remarkable with the creation of the implant pacemaker, by Wilson Greatbatch and William M. Chardack. It still remains as the most known medical implant device. Bioengineering plays an important role in technology and it has seen fast development.

Today, thousands of people around the world depend on implantable medical devices. These achievements result in the development of implantable medical devices with smaller dimensions, more safety, more complexity and more intelligence.

The choice of this thesis topic, *"Reducing Linearity Requirements for In-Body Communication in the Medical Implant Communication Service Band"*, is based on the intention of connecting technology and medical science. The progress of technology had a strong influence on the development of modern medicine. Today, medicine and technology are heavily interconnected. Even consumer electronic companies discovered the field of medical devices by implementing health applications in products like the Apple Watch. Taking this into account, the connection between telecommunication and bioengineering will be the next step in this development. We will see the emergence of new applications and products being invented by both the consumer electronics sector as well as the medical sector. The technological dream of a ubiquitous internet linking all our devices which we use, carry or may have implemented in our bodies is just about to become reality.

1.1 Goals of this Thesis

In this thesis two types of modulations– a $\frac{\pi}{8}$ - differential 8-phase shift keying (D8PSK) and a continuous phase modulation (CPM) – will be investigated. The choice of a $\frac{\pi}{8}$ - D8PSK modulation is related to the fact that the physical-layer (PHY) in the Institute of Electrical and Electronics Engineers (IEEE) 802.15.6 standard uses this modulation as a format for the highest bit rate. In order to conclude which modulation will use a cheaper and a simpler power amplifier (PA), which usually has a highly nonlinear characteristic. Supposedly a CPM is a good option. The simulation will prove this theory.

Those modulations will be compared in terms of power efficiency, linearity requirements and implementation complexity.

For that intention the medical implant communication service band (MICS), channel modeling for a body area network (BAN), nonlinear effects in PA, CPM and signal to noise power ratio (SNR) are going to be approached in detail along this thesis. An investigation of self and adjacent-channel interference by power spectral density (PSD)

calculations for both modulation schemes is also explored, as well as simulations of the bit error rate (BER) along the channel model.

The thesis concluded with an explanation of which modulation has a better performance in terms of power efficiency, linearity requirements and implementation complexity in terms of costs and efficiency.

1.2 Thesis Structure

This thesis is divided in six chapters. The first chapter comprises of a brief introduction about the motivation and the choise of this thesis topic.

Chapter two approaches the technological evolution discussed along this thesis. It starts with a brief technological history, followed by an explanation of a body area network (BAN) and MICS. It ends with the standardization of the IEEE 802.15.6 which defines the PHY structure.

Chapter three approaches the theoretical background. It starts with an explanation of power amplifiers (PA), followed by the channel model and a theoretical explanation of the two modulations studied.

In chapter four the MATLAB simulation is discussed from the view of the transmitter, the channel modelling and the receiver.

Chapter five explores the system performance and the final results.

The thesis ends with a general conclusion in chapter six. It summarizes the achieved results and draws the final conclusions. Furthermore, recommendations and future studies are presented.

2 Technology Evolution

This chapter approaches a brief introduction of biomedical engineering history, the theory of BAN, MICS and an explanation of the standardization used along this thesis.

The BAN testing represents an important role in the medical area. A wireless body network will emerge as a key technology providing realtime health monitoring and diagnosis of many life threatening diseases in the comming years. It can be used in, on or near the human body to enable medical problems, consumer electronics and personal communication.

MICS is a fairly new standard and plays an important role in implanted medical devices. It is an ultra-low power mobile radio service for transmitting data in support of diagnostic or therapeutic functions associated with implanted medical devices. In 1999, the Federal Communications Commission (FCC) allocated the 402-405 MHz frequency band for MICS operations.

Further ahead in this chapter will be the description of the IEEE 802.15.6 standard and its usage. This standard defines both PHY and MAC layers designed to satisfy the BAN needs. It can use existing industrial, scientific and medical (ISM) bands as well as MICS frequency bands approved by national medical and regulatory authorities. The PHY will be explained in more detail.

2.1 History of the Technology

During the 1950s, biomedical engineering was established as a discipline with multidisciplinary and professional teams. This decade was also remarkable for its biomedical technologies advances [Neb02].

Biomedical engineering is one of the technology fields which has been growing fast since 1950. Medical imaging, cardiac pacemakers, artificial limbs and some computer analysis of the human activity such as X-ray, the electrocardiogram, the electroencephalogram or the magnetic resonance imaging are some examples which defined the use of the principles and techniques of engineering to solve the problems in biology and medicine [Neb02].

Hermann von Helmholtz was a German physician and physicist who made significant contributions to physiology, optics, electrodynamics, mathematics and meteorology, during the 19th century. He may well be considered as one of the first biomedical engineers who invented the ophthalmoscope and the ophthalmometer. The ophtalmoscope can be used to examine retinal blood vessels which leads to high blood pressure and an arterial disease may occur as well. The ophtalmoscope remains one of the most important instruments for a physician as well as the ophthalmometer, which is an instrument for mesuring the curvature of the anterior surface of the cornea [Wil15]. Helmholtz determined the velocity of the nerve pulse transmission and he developed the basic physics for understanding fields in a volume conductor produced by bioelectric sources. He also studied the mechanism of hearing and created the Helmholtz resonator [Neb02]. These examples show, how biomedicine was influenced by the field of engineering, especially through instrumentation – for measuring and imaging [Neb02].

Transistors started to be commercially available in the 50s and were immediately used in biomedical applications. During the 1960s, when computers started to be widely available for scientists and engineers, they started to assist the progress of biomedical research. Particularly, in the field of cardiology, the technology has seen more extensive

use. It marked the beginning of a new era and therefore the beginning of modern biomedical research [Neb02]. At this time, Biomedical engineering had two faces in medical practice. On the one hand it has been seen as a problem because of its high costs for health care applications, while on the other hand biomedical engineering was a significant improvement, which provided much better diagnostic methods for patients.

The first mechanical heart valves were implanted in 1960 and quickly grew in their use. Bernard Lown, a cardiologist, developed the direct-current defibrillator, in 1962. Pacemakers became more common at this time thanks to Wilson Greatbatch, who accomplished the design and construction of an inhibited demand pacemaker in 1965. This new device only worked when needed [Neb02]. This pacemaker prototype automatically detected heart arrhythmias (asynchronous beats) and stopped the pulse output, not interfering with the patients own beats rhythms [Cha81]. Wilsons prototype led to the "Medtronic Model 5841", the first pacemaker to be commercialized [Neb02].

In 1970, J.C. Schuder and his team successfully implanted an independent defibrillator for the first time in history [Sch+70]. A rechargeable cardiac pacemaker was marketed between 1973 and 1978, and it has been successfully used in hundreds of patients. Researchers even developed a pacemaker powered by nuclear energy [Neb02]. The introduction of a lithium battery in Wilson Greatbatchs pacemaker led to the discontinuation of the nuclear and rechargeable pacemaker.

In the end of 1970s, Robert Javik and Wihelm Kolf, both researchers at the University of Utah, developed several artificial hearts and tested two of them, the Jarvik 5 and Jarvik 7 [Neb02] [Gri+87].

The usage of microprocessors in medical implant devices started to be a common practice during the 1970s. This new implementation allowed the usage of other electronical techniques for pain control, in external devices or implantable devices. The spinal cord stimulation (SCS), used for chronic pain, was another medical implant device with a major contribution to the medical world.

The evolution of electronical engineering shortly adapted to the arrival of microcircuits, which transformed the world of medical equipment and devices. Making them

smaller and more economic in both production and usage led to a breakthrough. In 1984, the Food and Drug Administration (FDA) approved the cochlear implant, which assembles a small, complex electronic device that can help to provide a sense of sound to a person who is profoundly deaf or severely hard-of-hearing. This implant consists of an external part that sits behind the ear and a second part that is surgically placed under the skin as shown in figure 2.1. The signals generated by the implant are sent through the way of the auditory nerve to the brain, which recognizes the signals as sound. Basically this implant is connected through electrodes in the cochlea [GR94].

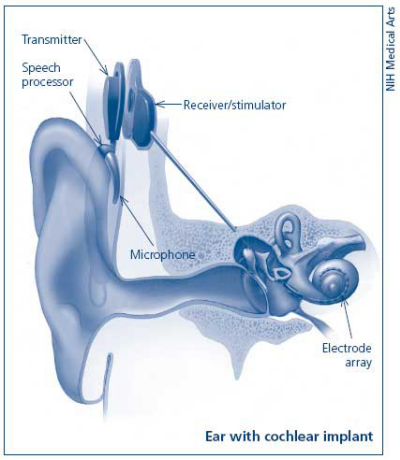

Figure 2.1: Ear with cochlear implant [NIH Medical Arts]

The most highly developed application of medical engineering was the radiology technology. In 1913, William Coolidge at General Electric developed some key technologies including improved X-Ray tubes, notably the high-vacuum hot-cathode tube and the means of visualizing soft tissues [Neb02]. Around the turn of the century, it has been discovered that ingestion of radio-opaque bismuth compounds made parts of the digestive tract visible in X-ray images. In the late of 1920s, the Portuguese researchers Egas Moniz and Dos Santos developed the so-called angiography, which means the X-ray visualization of blood vessels after injection of a radio-opaque substance [Neb02].

In the 1990s, the FDA approved a brain implant medical device for the first time. This marked a breakthrough in the area of implantable devices. The following commer-

cialization of a tremor control device for the Parkinson disease supported the momentun for implanted medical devices. The implanted impulse generator, placed inside the chest of a patient, sends signals to an electrode inside the thalamus.

Nowadays, biomedical engineering holds a prominent place as a way of improving medical diagnosis and treatment. Today, thousands of people around the world depend on implantable medical devices [Neb02].

Surgeries based in catheters begin to decline and open a space to get filled by other technological improvements. Invasive tools are being gradually replaced by smaller and more sophisticated devices, which can operate remotely through multiple electrodes, radio frequency (RF) transmitters and image sensors [Neb02]. On the other hand the evolution in the computing industry has facilitated mathematical modeling, enabling quantitative estimates of models that idealize the biological mechanisms instead of the empirical statistical substitutes [KN12].

2.2 Introduction to Body Area Communications

> "The ever-advancing miniaturization and the low power consumption of electronic devices, combined with recent developments in wireless communication is leading to a rapidly increasing demand for wireless communication in the human body area."
>
> Jianqing Wang
> Qiong Wang
> *[WW12, p. 1]*

In the human BAN various communication services should be located on, in or near to the human body in order to achieve a short range wireless communication or a small-scaled network to share data, reduce functional redundancies and to allow new services [WW12]. With those devices located along the human body the BAN can provide new possibilities in medical services, healthcare and consumer electronics applications.

BAN can also be named as a wireless body area network (WBAN) or body sensor network (BSN). The implant sensor can be placed either under the skin, or at a predetermined side in the human body in a fixed position, through wearable-technologies or accompanied devices which humans can carry in different positions [Pos09].

In 1995, the development of WBAN technology started with the idea of using wireless personal area network (WPAN) technologies which operate in the body area with radio frequency to provide a wireless network of wearable and human body implanted sensors and/or devices. A WBAN system can use WPAN wireless technologies as gateways to reach longer ranges. Over these gateways, devices can connect the wearable devices

mounted on to the human body through the Internet. Since the BAN field is an interdisciplinary area, which might allow reasonable and continuous health monitoring with real-time updates of medical records through the Internet, medical professionals can access patient data online using the Internet independently of the patients location. This is just one of many use cases a WBAN could provide [Pos09] [WW12] [FBB08].

Hence, the BAN can be divided into wearable BAN and implant BAN according to its location on or inside the human body where it operates. By definition, the wearable BAN communication contains all the communcation device used on the human body, the most known example of this BAN application is the Ericsson mobile health remote patient monitoring. The implant BAN communication shows heavy attenuation characteristics. It has some in-body devices which commmunicate with on- or off-body devices. Due to these different operating environments and characteristics, wearable BAN and implants may require different technologies for implementation, while a single solution for both is desired [WW12] [FBB08].

There are some requirements which should be considered because BAN operates in or near the human body and it focuses on personal information. Requirements such high data rate for real time transmission, extremely low consumption power for long-term use and a high quality of service to keep a highly reliable communication link should be considered [WW12].

In BAN communications the human body is used as a transmission medium, which changes completely the characteristics of the channel and also introduces a safety issue. BAN applies a higher safety priority to the human body than other wireless communication techniques. Therefore, these effects also interfere with the transmitting and receiving antennas because of the close vicinity of these sensors and the human body area. Parameters like specific absorption rate (SAR) need to be taken into consideration to protect the human tissues. SAR is a measure of the maximum energy absorbed by a unit of mass of exposed tissue of a human body using RF electromagnetic fields [WW12].

In the beginning of the 21st century, the term BAN has been associated to systems where communication entirely happened within, on and in the immediate proximity of a

human body. Therefore BAN attracted the attention of healthcare applications such as, healthcare monitoring in hospitals and at home as well as healthcare monitoring in a car; also for medical applications such as, medical diagnoses and treatment, to provide assistance to people with disabilities, consumer electronics and user identification. Those applications can take a continuous measure and transmit a vital sign or body physiological data to facilitate remote monitoring for the purposes of healthcare services, assistance for people with disabilities and entertainment or user identification [WW12] [FBB08].

Figure 2.2 shows where Medical Body Area Networks are using optimized wireless connections with low power consumption and low data rate due to the fact of the close proximity on or inside the human body. To meet such a broad range of data rates, different frequency bands may be required to find the best fit for these requirements [WW12].

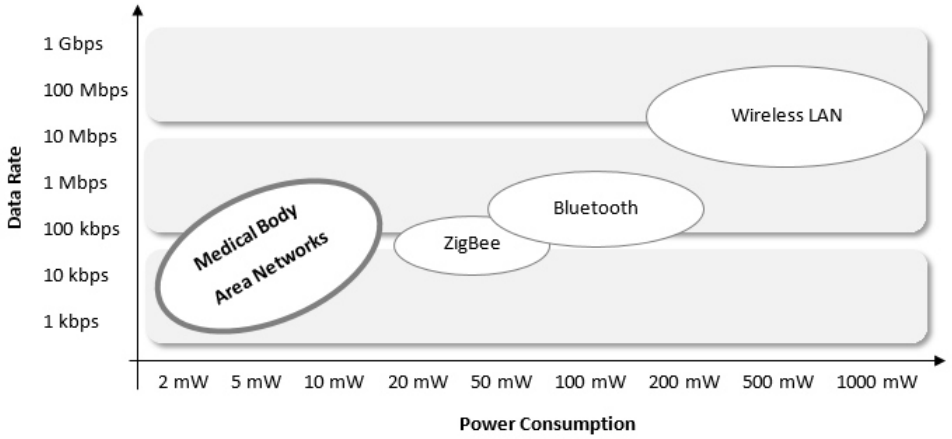

Figure 2.2: Comparison of the requirements between body area communication and other short range communications

2.3 Medical Implant Communication Service Band

The Medical Implant Communication Service (MICS) is a short-range, ultra-low power, unlicensed, wireless link to connect low-power implanted medical devices with monitoring and control equipment, mobile radio service for transmitting data in support of diagnostic or therapeutic functions associated with implanted medical devices [Sav+05].

In 1999, the United States Federal Communications Commission (FCC) defined that the frequency of the MICS band spans around 402-405MHz. These frequencies have conducive propagation characteristics in the human body and do not cause serious interference to other radio operations in the same band, creating a reasonable signal propagation.

It's important to note that we are only allowed to use quite limited transmit power in order to reduce the risks of the interference with other users of the same band. Therefore, the permissible maximum transmitting power in the MICS band is very low. The equivalent isotropically radiated power (EIRP) is allowed to be maximum at -16 dBm. Another drawback of the MICS band is that the 3 MHz frequency band cannot be used in full extend for a single transmit channel. The allowance extends to the use of 300kHz bandwidth. Thus, a high data rate is difficult because its limited bandwidth constraints the communication devices to low data transmission rates, even with sophisticated modulation schemes, data rates exceeding 1 MByte per second are hardly achievable. Although, the MICS band offers a good propagation behavior through human tissues and enables the use of reasonable sized antennas [Cha+13].

The MICS band also allows bi-directional radio communication in medical implant devices such as implantable cardioverter defibrillators, neuro-stimulators, hearing aids, automated drug delivery systems and cardiac pacemakers, as shown in figure 2.3. The MICS band technique allows the establishment of a wireless link between an in-body medical device and on- or near-body monitoring and control equipment [GR94].

The low attenuation of the MICS band compared with the ultra wide-band (UWB) signal when the signal broadcasts through the human body is the main benefit.

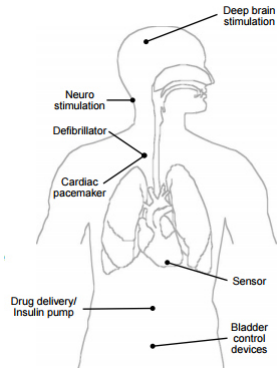

Figure 2.3: Medical Implant Communication Service Applications in the Human Body [Sem15]

This aspect makes the MICS band a promising candidate, especially for in-body communications [WW12].

Due to the ultra-low power characteristic of MICS devices, in Japan, the emission of MICS devices is up to 0.01 Watt for transmitting power consumption. A considerable change of the maximum transmitting power might represent a significantly increase to the usefulness of this frequency band. Additionally, the wireless medical telemetry system (WMTS) is assigned to 420-430 and 440-450 MHz. WMTS devices are also classified as specific low power equipment, which exhibit potential for use in BAN [WW12].

In 2009, the MICS band was expanded to 401-406MHz and called MedRadio as a response to the emerging field of neuro-recording, neuro-stimulation and neuro-modulation devices with their significantly increased data rates [Rit+14].

In 2011, the Alfred Mann Foundation filed a petition to expand frequency range further. This is currently installed roughly between 410 and 450Mhz, where the usable bandwidth will be extended to 6MHz. This allows data rates of more than 10 MByte per second. Note that this band is currently not internationally approved [Rit+14].

The MICS band was introduced through the traditional implants which use inductive links, limited range, low frequency and are not user friendly for home monitoring; need for higher data rates in order to upload the patients gathered data from the medical implant device's memory to the base station for analysis; need for longer range in order to

simplify the home-motoring for elderly, locate the base station outside of the sterile field during surgery; and competitive pressures of the medical device industry.

In the tissue properties, we face very large attenuation for UWB frequencies in the Gigahertz range. Thus, it is difficult to achieve deep implantation together with high data rates.

2.4 Standardization (IEEE 802.15.6)

The Standards Committee of the IEEE 802.15.6, is an international organization which develops international standards for wireless communications. Its scope is to cover not only the medical healthcare applications but also consumer electronics applications. The large scope of applications and wide range of technical requirements, however, mean the standard allows multiple physical layers (PHY) [WW12].

The IEEE Standard for local and metropolitan area networks Part. 15:6: Wireless Body Area Networks (IEEE Std 802.15.6-2012) was approved in February 2012. In the introduction it is stated that:

"IEEE Std 802.15.6-2012 is a standard for short-range, wireless communications in the vicinity of, or inside, a human body (but not limited to humans). It uses ISM and other bands as well as frequency bands in compliance with applicable medical and communication regulatory authorities. It allows devices to operate on very low transmit power for safety to minimize the specific absorption rate (SAR) into the body and increase the battery life. It supports quality of service (QoS), for example, to provide for emergency messaging. Since some communication can carry sensitive information, it also provides for strong security." [WW12, p. 11]

This IEEE Standard is an excellent solution for healthcare applications supported by electronic processes and communication.

In general, the main physical layer proposals include the narrowband (NB) phys-

ical layer in the MICS band, the UWB physical layer as well as the human body communications (HBC) band physical layer. It also defines a medium access control (MAC) protocol that controls the access to the channel [WW12]. The physical layer and the MAC layer protocols are used for communication between an implanted sensor and an on-body base station in the MICS band.

Following the IEEE Standard for local and metropolitan area networks, Part. 15:6: Wireless Body Area Networks (IEEE Std 802.15.6-2012), it uses a narrowband physical layer specification, which is responsible for the activation and deactivation of the radio transceiver, clear channel assessment (CCA) within the current channel and data transmission and reception.

2.4.1 Physical Layer of IEEE Std. 802.15.6

The physical layer or layer one is the first lowest layer of the open systems interconnection (OSI) model. OSI is a reference model for how applications can communicate over a network; it defines a seven-layer-framework to implement protocols for network communication.

The physical layer deals with the transmission of raw bits between different devices and supports electrical or mechanical interfaces connected over a physical medium for synchronized communication. The bit stream might be grouped into codewords or symbols and converted to a physical signal that is transmitted over a hardware transmission medium. It can specify the shapes and properties of the electrical connectors, the modulation schemes to use and the frequencies to broadcast. A PHY can provide an electrical, mechanical and procedural interface to the transmission medium [Iye+11].

The choice of the PHY depends on the target application, such as medical/non-medical, in-, on- or near-body. As mentioned before, the IEEE Std. 802.15.6 uses a NB PHY [Lee+09]. The NB PHY is responsible for the activation and deactivation of the radio transceiver, CCA within the current channel and data transmission and reception [IEE12].

It also provides a method for transforming a physical-layer service data unit (PSDU) into a physical-layer protocol data unit (PPDU).

During the transmission, the PSDU should be preceded by a PHY-layer preamble and a PHY-layer header in order to create the PPDU. At the receiver, the PHY-layer preamble and PHY-layer header aid in the demodulation, decoding and delivery of the PSDU [IEE12].

Figure 2.4 shows the PPDU which is a frame structure inside the PHY. It is formed of three main components: the physical-layer service convergence protocol (PLCP) preamble, the PLCP header and the PSDU.

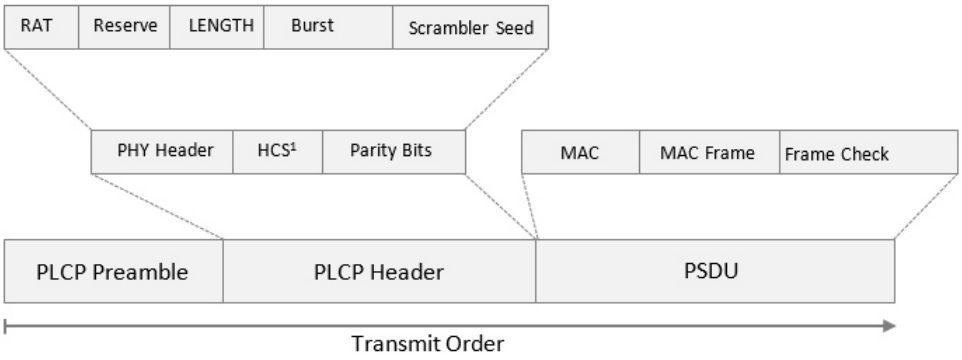

Figure 2.4: Standard physical frame structure [IEE12]

Physical-Layer Service Convergence Protocol Preamble and Header

As can be observed in figure 2.4, the PLCP preamble is the first component of the PPDU. The PLCP preamble is a bit sequence with the purpose of assisting the receiver in the timing synchronization and carrier-offset recovery. The MAC and PHY parameters are used to determine the PLCP format in the first step of encoding the PLCP preamble [IEE12] [IEE15].

The PLCP header is the second main component of the PPDU. Its purpose is to convey the information about the PHY and MAC-layer parameters that is needed at the receiver in order to aid in the decoding of the PSDU [IEE12].

The MAC-layer communicates with the PLCP through a service access point (SAP). When the PLCP header receives the instruction from the MAC-layer, the PLCP prepares the MAC protocol data units (MPDUs) for transmission. That means the octets (eight bits) will be send through the PSDU to the MAC-layer, indicating a successful received message; once the last octet group is sent, the PLCP sends a message, indicating that it has received the final octet to continue the procedure. The PLCP minimizes the dependence of the MAC-layer by mapping MPDUs into a frame format suitable for transmission by the physical medium dependent (PMD). The PLCP also delivers incoming frames from the wireless medium to the MAC-layer [IEE15].

The PLCP header can be decomposed into a PHY-layer header, a header check sequence (HCS)[1] and parity bits, which can be split into a rate field, reserved bits, a length, a burst mode field and a scrambler seed field as seen in figure 2.4. The parity bits use a Bose-Chaudhuri-Hocquenghem (BCH) code, which consists in the addition of bits in order to improve the robustness of the PLCP header. The PLCP header has to be transmitted using the given header data rate in the operating frequency band [IEE12].

Physical-Layer Service Data Unit

The last component of the PPDU is PSDU. It is formed by coupling the MAC-layer header with the MAC-layer frame body and frame check sequence (FCS). Before the PSDU being scrambled, it might be encoded and spread/interleaved. The PSDU should be transmitted using one of the data rates available in the operating frequency band [IEE12].

Once the packet is transmitted the PLCP preamble is the first to be sent, followed by the PLCP header and later by the PSDU. All multiple octet fields shall be transmitted with the least significant octet first and each octet must be transmitted with least significant bit (LSB) first [IEE12].

[1] HCS - Header check sequence

The main goal of this thesis is to research whether it is possible to use implanted sensors for the medical surveillance of patients. Since the human body is the environment where these systems will work, the MICS band needs to be evaluated for in-body communications.

The communication occurs between two devices, in this case between two sensors. One will be transmitting the information and the other one will be receiving this information. Our attention is focused on the transmission side. Consequently, the bits which are transmitted from the MAC-layer to the PHY will have more relevance.

As mentioned before, the PSDU sublayer contains the real data from the MAC layer, therefore our attention is captured on this sublayer in the following pages. It is crucial to always keep in mind that a compatible device should be able to support transmission and reception between 402 MHz and 405 MHz, being the allowed frequency interval for MICS band.

The PSDU is the last major component of the PPDU, it must be constructed as shown in figure 2.5. It shows the data flow on the sending end and the receiving end respectively in the upper and lower portion of the scheme.

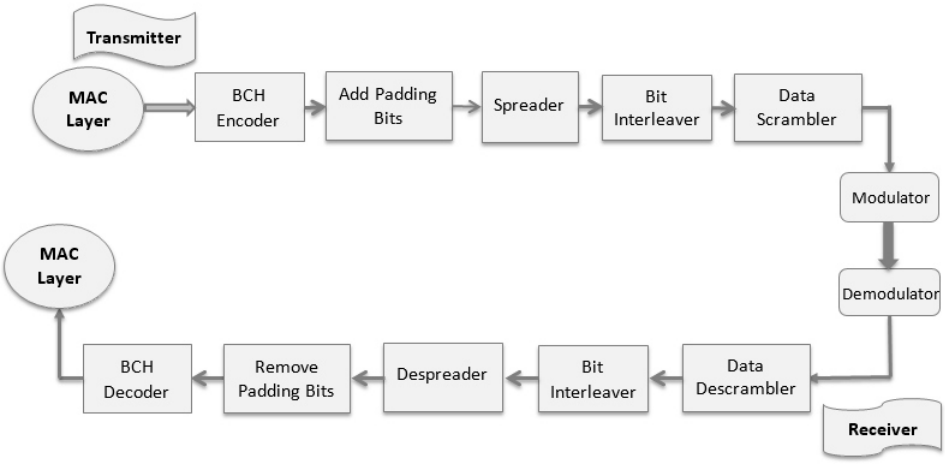

Figure 2.5: Block diagram of PSDU construction for transmission and reception [IEE12]

In order to use this universal block diagram of figure 2.5 for a PSDU in $\frac{\pi}{8}$ - D8PSK modulation some blocks can be excluded from it.

The pad bits will be appended after the BCH encoder to align the bit stream on a symbol boundary. The pad bits will not be taken into consideration as well as the data scrambler because the system generates automatically random bits. Consequently there is no need to align the bits, since they will be different all the time.

The spreading is the ratio between the transmission bandwidth and the original bandwidth. The spreading factor for $\frac{\pi}{8}$ - D8PSK modulation is $SpreadingFactor = 1$, as shown in table 2.1. If the spreading factor would be two, each input bit will be repeated two times along the block array. The lower the spreading factor, the more data payload a signal can convey on the radio interface.

The bit interleaver depends on the spreading factor. For this reason, it will not be considered for $\frac{\pi}{8}$ - D8PSK modulation. In the case of a spreading factor equal to two, the output of the spreader should be interleaved previous to the modulation to provide robustness against error propagation. The exact structure of the bit interleaver depends on the number of uncoded bits that will be transmitted on-air.

A side-stream scramble with polynomial $G(x) = 1 + x^2 + x^{12} + x^{13} + x^{14}$ is used to withen the PHY header and PSDU [Cro15]. Scrambling can facilitate the work of a timing recovery circuit, an automatic gain control and other adaptive circuits of the receiver. It eliminates the dependence of a signals power spectrum upon the actual transmitted data, making it more dispersed to meet maximum power spectral density requirements. Figure 2.6 shows a typical implementation of a side-stream scrambler. The output of the scrambler is generated as shown in equation (2.1) [IEE12] [Cro15].

$$x[n] = x[n-2] \oplus x[n-12] \oplus x[n-13] \oplus x[n-14] \tag{2.1}$$

Where $\oplus$ denote modulo-2 addition.

After excluding all the blocks mentioned before, the $\frac{\pi}{8}$ - D8PSK modulation will be using only the BCH encoder and the modulator blocks from the transmitter perspective (figure 2.7).

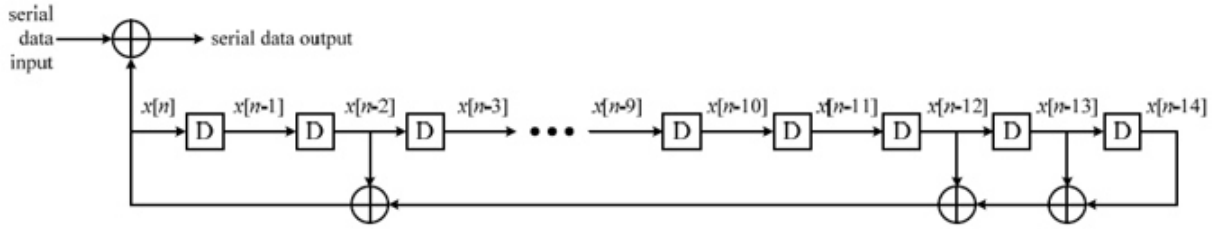

Figure 2.6: Block diagram of a side-stream scrambler [IEE12]

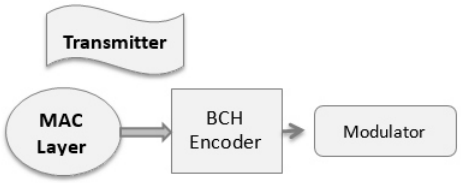

Figure 2.7: Block diagram of PSDU for transmission

A modulator is a device that performs modulation and a demodulator is a device that performs demodulation, so the inverse of modulation. In the telecommunications field, modulation is the process of varying one or more properties of a periodic waveform, called the carrier signal, with a modulated signal that usually contains the information which is needed to be transmitted.

For modulating and demodulating the signal, the symbols are mapped onto the appropriate constellation which is determined by the data rate dependent parameters for frequencies band between 402 MHz and 405 MHz. Those frequencies band are used in the IEEE Standards (Table 2.1). From this table can be observed that $\frac{\pi}{8}$- D8PSK modulation has a data rate of 455.4 kbits per second (bps), being that the reason for the investigation of this modulation in this study.

The BCH encoder for PSDU uses a code rate of 51/63, where 51 is the message length k, and 63 is the codeword length n. BCH$(63, 51)$ code is used to calculate error correcting codes attached to the PHY header and PSDU. It may be shortened in the case that the source bits are not a multiple of 51 [IEE12] [Cro15].

Table 2.1: Modulation parameters for PSDU [IEE12]

Packet Component	Modulation (M)	Symbol Rate = 1/Ts (kbps)	Code Rate (k/n)	Spreading Factor (S)	Pulse Shape	Information Data Rate (kbps)	Support
PSDU	$\frac{\pi}{2}$- DBPSK (M = 2)	187.5	51/63	2	SRRC	75.9	Mandatory
PSDU	$\frac{\pi}{2}$- DBPSK (M = 2)	187.5	51/63	1	SRRC	151.8	Mandatory
PSDU	$\frac{\pi}{4}$- DQPSK (M = 4)	187.5	51/63	1	SRRC	303.6	Mandatory
PSDU	$\frac{\pi}{8}$- D8PSK (M = 8)	187.5	51/63	1	SRRC	455.4	Optional

In this thesis the BCH code uses a Berlekamp-Massey algorithm and a binary Galois-field as will be described in the following chapter.

2.5 Summary

The conclusion from this chapter is that a BAN built upon 802.15.6 is an excellent solution for healthcare. Due to the fact this communication method is optimized for low power consumption. It is a term for healthcare practice supported by electronic processes and communication.

Is also important to keep in mind that the frequency range allowed in MICS is between 402-405 MHZ. These frequencies have conducive propagation characteristics in the human body and do not cause serious interference to other radio operations in the same band. MICS allows a bi-directional radio communication in medical implant devices. It uses a wireless link technique to connect in-body medical device with an on- or near- body monitoring and control equipment.

The standardization section gives a brief explanation about the used standard from an implementation perspective. In general, the standard defines three PHY, the NB, the UWB and the HBC layers. The selection of each PHY depends on the application.

On a NB PHY the attention is focused on a $\frac{\pi}{8}$ - D8PSK modulation. The standard also defines a MAC protocol that controls the access to the channel.

Is also important to keep in mind that the data rate of $\frac{\pi}{8}$- D8PSK modulation is 455.4 kbps, being that the reason for the investigation of this modulation in this study.

Since, in this thesis the attention is focused on the transmitter side, the PSDU sublayer, from the standard PHY frame structure is explored in detail. Due to the fact that it contains the real data from the MAC-layer. Therefore some blocks are excluded from the block diagram of PSDU, leaving only the MAC-layer, the BCH encoder and a modulator from the transmitter view. The BCH encoder for PSDU uses a code rate of BCH(51/63).

3 Concepts and Theory

This third chapter aproaches all the theoretical background needed to understand the concepts, required in this thesis. It starts for all the theory behind the BCH code used in chapter 2.

The characteristics of a wireless signal changes as it travels from the transmitter antenna to the receiver antenna. These characteristics depends upon the distance between the two antennas, the paths taken by the signal and the environment around the path. Since, the MICS works in a human body environment there are several influences which must be taken into consideration, such as, the tissues, the organs, the bones, the muscles and all the others parts of a human body. Thereby, a frequency of 402-405 MHz is used, as explainded in the previous chapter.

The received signal can be obtained directly from the transmitted signal, although if there is any other model, i.e. noise, between them it will change the receiver characteristics. This transmission medium model is called channel model.

Figure 3.1 represents a channel model communication.

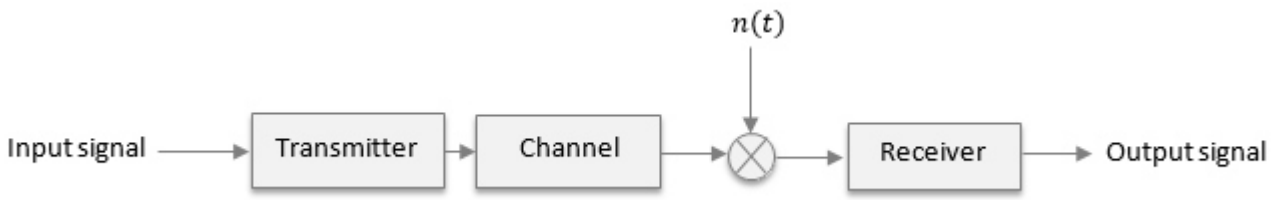

Figure 3.1: Channel model overview

In this channel model must be taken into consideration the type of pulse shape, the PA to use and the type of modulation – $\frac{\pi}{8}$ - D8PSK and CPM. This chapter approaches the theoretical background of these components.

Two types of modulations will be analyzed along this thesis and a brief explanation of them will be approached.

3.1 Bose-Chaudhuri-Hocquenghem codes

The BCH codes form a large class of multiple random error-correcting codes. The BCH codes are cyclic codes. In the end of 1950s and beginning of 1960s Alexis Hocquenghem, Ray Bose and D. K. Ray-Chaudhuri discovery the codes, without the decoding algorithms, independently [Zhe15].

A BCH encoder creates BCH code with a specific message, k and a codeword length, n. BCH code provides precise control over the number of correctable symbol errors during the code design, which is one of its significant features. A BCH encoder is also able to correct multiple bit errors. Another feature is the easy decoding via an algebraic method known as syndrome decoding. These features will be described in more detail later.

Once, the BCH code receives the multiplexed signals, simultaneously, each receiver can use the logical exclusive OR function (XOR) for computing them with the spreading code to get back to the original signal [Wal15]. Each transmitted signal crosses a noisy channel which adds noise to the information without our consent, corrupting the information to a degree related to the character and strength of the noise. Consequently, we will have a transmitted signal with noise appearance. Therefore the receivers will ignore the signals that are not correlated with the spreading code [Cro15] [Zhe15].

A BCH decoder follows four steps, the computation of the syndrome, the determination of an error locator polynomial, searching the roots of the error locator polynomial and determine the error magnitude at each error location by error-evaluator polynomial

(this one is just for nonbinary codes, which is not the case) [Han15]. The decoding procedure can be performed in time or frequency domains [Moo15] [Wal15].

The computation of the syndrome can be define by $S_j, 1 \leq j \leq 2t$. Considering $\alpha, \alpha^2, ..., \alpha^{2t}$ are the $2t$ consecutive roots of the generator polynomial for the BCH code, where α is an element in finite field $GF(q^m)$ with order n [Han15]. The received vector is denoted by $y(x)$, so the syndrome $S_j, 1 \leq j \leq 2t$, as follows:

$$\begin{aligned} S_j &= y(\alpha^j) = c(\alpha^j) + e(\alpha^j) = e(\alpha^j) \\ &= \sum_{i=0}^{n-1} e_i(\alpha^j) \\ &= \sum_{k=1}^{v} e_{i_k} \alpha^{i_k j} \end{aligned} \tag{3.1}$$

Where n is the codeword length, as mentioned before, and it is assumed that v errors occurred in locations corresponding to time indexes $i_1, i_2, ..., i_n$. The syndromes at the minimum polynomial can be calculated for α_j and $n > 1$ [Han15] [Wal15].

The roots of an error locator polynomial provide an indication of where the errors are. There are several different ways of finding the locator polynomial. For BCH codes, the used methods are the Petersons algorithm, the Berlekamp-Massey algorithm and Euclidean algorithm. In addition there are techniques based on the Galois-field Fourier transforms [Han15] [Moo15].

The Berlekamp-Massey algorithm builds the error locator polynomial. The polynomial coefficients satisfy a set of equations called the Newton identities [Han15] [Moo15].

The Newton's identity are given by equation 3.2 [Han15].

$$S_k = -\sum_{j=1}^{v} S_{k-j} \Lambda_j, \qquad k = v+1, v+2, ..., 2 \cdot v \tag{3.2}$$

This equation describes the output of a linear feedback shift register (LFSR) with coefficients $\Lambda_1, \Lambda_2, ..., \Lambda_v$. In order to find the Λ_j coefficients in a way that the LFSR generates the known sequence of syndromes [Moo15]. Note that finding the shortest number of coeffiecients of a LFSR is equivalent to find the error locator polynomial [Han15].

After decoding the error locator polynomial can be found through Berlekamp-Massey algorithm, as described above [Moo15].

3.2 Power Amplifier

Power amplifiers (PA) play an important role in the modern communications systems. They are used in wireless transmitters, broadcast transmitters and hi-fi audio equipment. It provides the transmission signal levels needed to overpass the loss between the transmitter and the receiver. Once PA is the last component of the transmitted channel model – placed before the antenna– consequently it implements the final amplification of the transmitted signal. In that way, when the signal reaches the receiver it can be received with the required distance and the desired quality [Lia+99] [MS15].

In consideration of the PA being the last component of the transmitted channel model, it is required that it deals with the highest power levels. Thus, the PA usually displays the utmost power consumption in the transmission channel, which means the efficiency of the system can be basically reduced to the efficiency of the PA. Moreover, this component intensively influences the quality of the output signal. When the PA works close to its nonlinear performance, it increases its influence on the quality of the output signal. Nevertheless, usually the amplifiers operate as linear devices under small signal conditions and become more nonlinear and distorting with the increase of the power consumption [MS15].

The efficiency of the amplifier increases with the increase of the output power. The system-level tradeoff between the power efficiency/high-performance and the high integration characteristics, is caused because the PA still a RF component that has not been totally integrated into the whole transceiver. This tradeoff can be limited and as a result the amplifier signal levels are shortened from the peak efficiency operating point [Lia+99] [MS15].

The complementary metal oxide semiconductor (CMOS) technology processes are known for the following advantages: low costs, high availability and integrity, among the integrated circuits (IC) technologies [MS15].

Although, for PA integration the silicon-based CMOS can be seen as the worst process. It still remains a challenge to achieve high-linearity. Therefore, the high-performance can be achieved by focusing on expensive processes, which prevent the PA from being implemented in low cost and highly integrated devices. Additionally, a high-performance PA is crucial because the PA power consumption can easily make up 50 percent of the overall power consumption of the tranceivers performance. This altogether means that PAs have a direct impact on transceiver performance [MS15].

Nevertheless, PAs also have some drawbacks. The required transmitted power and the losses associated to the amplifier inefficiency can be consume by the amplifier as a major fraction of the system power. Which can help to define the battery life for mobile communication systems [Lia+99].

The PA can change the transmitted signal characteristics. When a pulse shape with root raised cosine (RRC) filter is used in the channel model in order to isolate the effects in the solid state power amplifier (SSPA). The PA is followed by an introduction of additive white Gaussian noise (AWGN) in the signal frequency band, which creates unexpected frequencies in adjacent channels. This adjacent channel interference (ACI) is tightly controlled by the communications standard being used [Lia+99]. As will be shown in the following chapter.

A SSPA is an amplifier that uses field effect transistors to provide useful amplification at higher frequencies. It also provides a full complement of analog telemetry signals. SSPA operates in compression to maximize efficiency for constant envelope modulation but can be ordered with automatic level control (ALC) to maintain linear operation for modulation formats. The amplitude-to-phase transfer function (AM/PM) conversion of the SSPA is assumed to be small enough, so it can be ignored. The amplitude-to-amplitude transfer function (AM/AM) conversion fucntion can be described by a Rapp Model as a nonlinear amplifier, which will be discussed in more detail on the following pages [Rap91].

There are two types of modulation formats, the constant envelope modulation – as mentioned before – and the non-constant envelope modulation [Lia+99]. The constant envelope modulation provides significant advantages over the standard phase shift keying (PSK) forms of modulation.

All constant envelope modulations allow a transmitter PA at or near saturation levels. A constant envelope modulation has a fixed signal and is not affected by a non-linear amplifier transfer functionAM/AM. Although, it can contain AM/AM component in the modulated envelope, which requires a larger bandwidth than a non-constant envelope modulation. That might cause an ACI when there is a small carrier frequency separation between the adjacent channels [Lia+99].

In the non-constant envelope modulation, the signal is varying on time and the information can be modulated on the amplitude of carrier frequency, such as AM/AM. The power spectrum efficiency of this kind of modulation is always higher than a constant envelope modulation. These larger power amplifiers are less efficient, consume more primary power and generate more heat [Lia+99].

The following pages discuss the impact of a PA in terms of power consumption, the PA performance and a brief description of the importance of the peak to average power ratio (PAPR) in PA. PA metrics and the nonlinearity of a PA, which will be an important point in the following chapters.

3.2.1 The Impact of Power Amplifiers on Integrated Transceivers

The channel bandwidth, channel modulation, the frequency band and output power levels change from standard to standard in modern wireless regulations. Due to the fact that the power consumption of a PA in wireless transceiver has always been considered high [MS15]. As described before, the impact of the PA on the transceiver can vary with the use of a RRC filter in the channel model.

The communication range and the channel spectral efficiency are the two main system parameters that affect the PAs performance of a modern wireless standard. These

two parameters immediately correct the linear output power and PA efficiency, which are other two main aspects of PA [MS15].

Figure 3.2 shows a simplified block diagram of a generic RF transceiver. The transmitter baseband, the receiver baseband, the transmitter front-end, the receiver front-end and the synthesizer blocks are the main circuits on the block diagram. The transmitter and receiver baseband blocks are for signal processing, the transmitter front-end is responsible for the modulation and up-conversion, the receiver front-end is responsible for down-conversion and demodulation, and the synthesizer is responsible for the creation of the carrier frequency. The PA block amplifies the signal to produce the required RF transmit power to the antenna. The power consumption of the transceiver will comprise the power consumption of all these blocks [MS15].

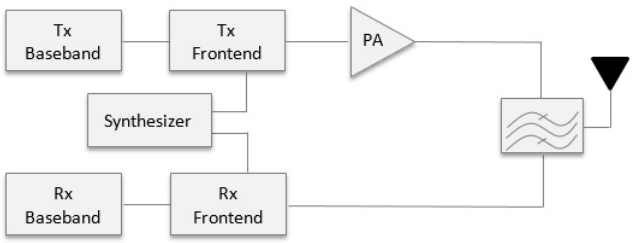

Figure 3.2: Transmitter simplified block diagram

Through this simplified scheme it is possible to quantify the impact of the PA on the transceiver side for actual wireless communication standards, given by the following equation [RP14].

$$PA_{impact} = \frac{P_{PA}}{P_T} \tag{3.3}$$

Where P_{PA} is the power consumption of the PA and P_T is the power consumption of the whole transceiver, including the PA. The impact depends on the output power levels used by each standard and consequently is not the same.

3.2.2 Power Amplifier Performance

As considered before the PA performance is mostly affected by the energy efficiency in limited channel bandwidths. Although, its impact not only affects the channel bandwidths but also the modulation, in order to increase the spectral efficiency (more bits per second per hertz of bandwidth) on the uplink data transmission [RP14].

Sometimes the transmitted signal has higher peak power values than the average, which means that the signal has a high peak to average power ratio (PAPR). This points us to the need of using amplifiers with highly linear characteristics, otherwise the excessive clipping of the signal would lead to a distortion of the transmitted signal and out-of-band radiation. Though these consequences depend on the terms of maximum limits for error vector magnitude (EVM) [1] and adjacent channel leakage ratio (ACLR) of the standard. However, there are some wireless standards which that requires a special attention to the higher PAPRs values. The IEEE 802.15.6 Standard is one of these examples [RP14].

A PA is directly affected by high PAPRs in terms of linearity requirements and in terms of efficiency by the component. Usually the PA achieves the maximum efficiency at maximum power. Although, for a high transceiver PAPR the maximum power level will be only achieved for short time intervals [RP14].

3.2.3 Power Amplifier Fundamentals: Metrics

The PA metrics can be combined into two main groups: linearity and efficiency. AM/AM and AM/PM distortion are two significant effects in PAs at high output power levels. The AM/AM distortion refers to the amplitude distortion of any amplifier that is driven in a linear or nonlinear condition. The AM/PM distortion refers to the change in the phase difference between the output and the input signals as a function of the input signal level. It is seen that both distortion effects can be measured with high accuracy [MS15] [SDC09].

[1] EVM - is a measurement of modulator or demodulator performance in the presence of impairments

As mentioned in the beginning of this section the PAs are designed to be in the final stage of a transmitter for a specific communication standard. Therefore, even when the AM/AM or AM/PM distortion parameters are useful for evaluating the performance of a PA, it is more important to know if the PA will fulfill the specifications imposed by the used standard. The fact that the modulation in a digital channel vary with a high PAPR is seen as a disadvantage. Because it has a direct impact on the PAs requirements in terms of linearity. These standards set the linearity requirements of the transmitter by specifying the maximum permissible out-of-band emissions. These emissions are limited by the adjacent channel leakage ratio (ACLR) and the spectrum emission mask [MS15].

Testing the PA with realistic channels allows for the determination of the actual efficiency and the power levels that the PA can handle for the specific standard while complying with requirements like the PSD mask or EVM.

The PSD describes how the power of a signal is distributed over the different frequency. The power can be physical power or defined as the squared value of the signal, which is used, more often, for abstract signals. The PSD is obtained by computing the Fourier Transform of a signal with the autocorrelation function. PSD is very useful for knowing frequencies and to compare the variance of a process by integrating over frequency [int15].

In the following chapters the PSD will be used as an an important tool for the choice of some parameters.

3.2.4 Nonlinear Model of a Power Amplifier

In 1980, Afred J. Cann proposed an instantaneous nonlinearity model with variable knee sharpness. In 1996, Litva and Lo found out that it gave incorrect results for a two-tone intermodulation test, and in 2000, Loyka diagnosed the reason: nonanalyticity. Further studies showed that no problem exists with typical real-world signals. Nevertheless, Cann present a new model that eliminates the problem entirely [Can12]. As mentioned before usually the amplifiers operate as a linear device under small signal conditions and

become more nonlinear and distorting with increasing drive level.

Sometimes the nonlinearity is used to achieve a desired effect, such as the synchronization of two oscillators. In many cases, the degree of nonlinearity must be chosen carefully: strong enough to ensure the desired effect but not too strong that chaos results [Lia+99] [Can12].

The characteristics of nonlinearities are usually measured at only a discrete set of points. Regularly a small nonlinearity of an amplifier operated bellow saturation is a huge concern, because it causes harmonic distortion and intermodulation distortion [Can12].

In 1980, Cann proposed an instantaneous nonlinearity model with variable knee sharpness seen as a convenient feature, although it gave wrong results for intermodulation products (IMP) in a two tone test because it was not analytic at zero. Later on was proven that this issue is particular for the two-tone test and does not happen in real world signals [Can12].

Cann made a comparison between the new model and other models in literature. But because these are all envelope models, the comparison needed a discussion of envelope models, which is used in a different way from instantaneous models. He wrote about the behavioral models and not about the circuit models. A broadband system required the use of an instantaneous model also called a discrete model, which takes care of all the entire waveform and can reproduce harmonics and even-order IMPs .

As mentioned before the IEEE Std. 802.15.6 uses a narrowband PHY. It uses a lowpass model, also called an envelope model which makes the computation more economical because it can use a lower sampling rate. A Narrowband system is generally defined as one whose bandwidth is considerably less than the center frequency [Can12]. So Cann said that there is a broad area in which both instantaneous and envelope models can be used while producing the same results.

Cann defends that nonlinearity is important in the low-level stages of receivers, where intermodulation can give rise to strong-signal interference. The recent work cares about power amplifier because communication links have proliferated in which both power consumption and spectrum space are at a premium. It is recommended to operate the

power amplifier well into saturation for maximum power efficiency. On the other hand, to operate well below saturation to minimize intermodulation distortion, which causes interference among the channels and spectrum regrowth [Can12].

In 1989, Cann analyzed several models like the original model for an instantaneous model with adjustable knee sharpness. Later on he analyzed the new model which was inspired by the observation that the magnitude portion of the Bode plot of the transfer function of a simple lead network has the required kind of shape. Envelope models such as envelope representation of bandpass signals and envelope model characteristics. In 1981, Saleh proposed a closed-form model for traveling-wave-tube amplifier. In 1991, Rapp proposed a closed-form envelope model with adjustable knee sharpness for SSPAs . The new model was originally developed as an instantaneous model. It can also be used as an enveloped model. The Ghorbani Model as well as the White Model have also been studied by Cann.

Therefore, for both modulations – $\frac{\pi}{8}$ - acD8PSK and CPM – the Rapp Model will be the nonlinear model of a power amplifier used in the simulation. In the chapter 5 this model will be explained in more detail. This model is characterized by having an adjustable knee sharpness and is able to provide any sharpness desired. Once this model is not analytic at zero, it must be used with caution and only for signal waveforms that are sufficiently complex to have a wide amplitude distribution [Can12].

3.3 Channel Model

A channel model can be a transmission medium and is used to convey information signals from one or several transmitters to one or several receivers. The channel has a certain capacity for transmitting information, which is often measured by its bandwidth in Hertz or its data rate in bps. It is the initial step to explore and investigate in body area communication [WW12].

Depending of the position of the transmitter and receiver devices a body area channel can be classified as wearable channels and implant channels. The main difference between these two body area channels is that the wearable channels have all the devices on body, whereas the implant channels have some devices inside the body which communicate with on-/off- body devices. An implanted pacemaker in the chest is an example of an implant channel, due to its communication with an on- or off-body device [WW12].

A wearable channel can be classified as a line of sight (LOS) or a non-line of sight (NLOS). It depends on the propagation of the electromagnetic waves between the two devices. For example, when a device is on the chest of the body and the other device is on the front, this situation is characterized as a LOS propagation because the electromagnetic waves will propagate in the normal way without any losses caused by diffraction around the body [WW12].

Although, the wave propagation characteristics in the human body environment pose many challenges to the future of the human implants. There are absorption phenomena in human body due to dielectric propagation losses of the body tissues, scattering because of the heterogeneous nature of the body tissues as well as diffraction and creeping waves exist along the body surface. The excitation of surface and space waves from radiating antennas mounted on the body can have a large impact on the performance of co-site body-centric antenna systems. Besides, the existence of multiple antennas on the body can lead to an unexpected coupling due to creeping wave interaction. However the finite difference time domain (FDTD) method helped to study, in more detail, the problem

of body-centric antenna systems [WW12] [BM15a].

Moreover, the fact that the human body might have different postures during the communication period between the two devices, multiple paths are created between the transmitter and receiver so that a transmitted signal can traverse. Consequently, the received signal may end up with biased results, such as, signal delay, time-varying, superimposition of several attenuated or eventually with distorted replicas of a transmitted signal. That must be taken into consideration in a on-body implant [WW12].

The dominant channel characteristics change for different body area channels, an on-body channel suffers more from multipath fading and shadowing due to body postures and movements than an in-body channel, whereas an in-body channel experiences a higher signal loss during the transmission [WW12].

According to that, a channel model needs to merge the wave propagation characteristics in the body area with the different environment conditions, such as different channel types (in-/on- body) and different frequency bands (UWB, MICS and HBC).

3.3.1 Path Loss Model

Path loss models describe the signal attenuation between a transmitter and a receiver antenna as a function of the propagation distance and other parameters. The path loss happens as a result of many effects, such as free-space loss, refraction, diffraction, reflection, aperture-medium coupling loss and absorption. It can be divided in four types, free-space path loss, on-body UWB path loss, in-body UWB path loss, in-body MICS band path loss, HBC band path loss and equivalent circuit expression (equivalent circuit expression (ECE)) [WW12] [Say+09].

Considering that the main topic of this thesis is studying the in-body communication in the MICS band, the path loss will be approached in detail in the following pages [WW12].

Since MICS is characterized for the use of narrowband signals, its path loss characteristics result on the ratio of the received average power and the transmitted average

power, rather than the ratio of energy [WW12].

So, path loss at a distance d from the transmitting antenna is given by the equation (3.4),

$$PL(d) = \frac{G_r P_T}{P_R(d)} \tag{3.4}$$

Where PL is the linear path loss, G_r is the receiver antenna gain, P_T the transmit power and P_R the receiver power. Usually the wireless systems channel models do not include the transmitter antenna gain, but for MICS band the transmitted antenna needs to be considered as a part of the channel [WW12] [Say+09].

In wireless communications, the path loss is usually expressed in decibels. It can be represented as PL_dB, shown by the following equation (3.5),

$$PL(d_{dB}) = PL(d_0) + 10 * n * log_{10}\left(\frac{d}{d_0}\right) + S, d \geq d_0 \tag{3.5}$$

where d_0 is the reference distance, n is the path loss exponent which depends on the environment where RF signal is spreading through, d is the distance between the transmitter and the receiver, and S is the random scatter around the mean. S represents the deviation in dB caused by different materials and antenna gain in different directions [WW12] [Say+09]. In chapter 5 all the values used for calculating the path loss will be shown.

The path loss can be modelled in two different ways. The first method is finding values for the parameters (i.e. PL_d0, n and S) for the entire data set which then get serarated into implant-to-implant and implant-to-body surface sets. The second method consists of the separation of set parameters (i.e. PL_d0, n and S) for deep tissue implants in contrast to near-surface implants. When there are no obstacles, a free path loss can be added to these models in order to justify the additional loss which the implant signal go through once it leaves the body. On the other side, when the body has adjacent obstacles in the surroundings, the loss could occur as well as some changes need to be made to the model accordingly [Say+09] [Cha+13].

In order to understand the RF channel characteristics inside the human body, an appropriate design platform would be very helpful. Regarding the complexity of the propagation environment surrounding a medical implant, an innovative three-dimensional virtual reality simulation platform aimed at RF propagation study in BANs, was developed at the information technology laboratory of the National Institute of Standard and Technology (NIST). The propagation engine is a three-dimensional full-wave electromagnetic field simulator, the 3D immersive, visualization platform and a body surface antenna, as shown in figure 3.3 [Say+09] [Cha+13].

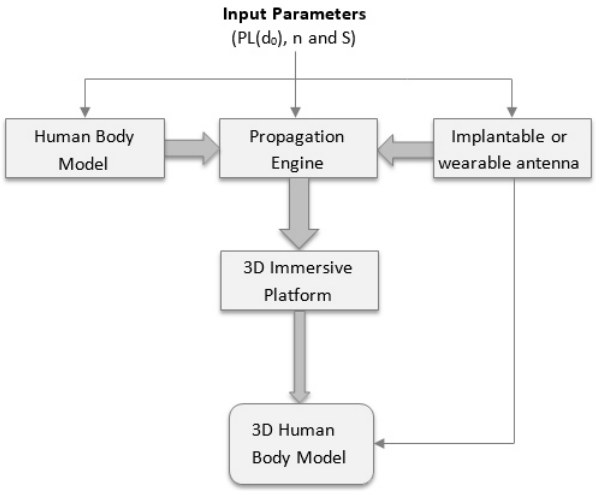

Figure 3.3: System block diagram [Say+09]

The propagation engine allows computing a variety of different electromagnetic quantities such as the magnitude of electric and magnetic fields or SAR. The 3D immersive platform includes several important components: three orthogonal screens that provide the visual display, the motion tracked stereoscope glasses and the handheld motion tracked input device. The screens are used to display a single 3D stereo scene. The scene is updated based on the position of the user as determined by the motion tracker. This allows the system to present to the user a 3D virtual world within which the user can move and interact with the virtual objects. The 3D human body model includes frequency dependent dielectric properties of more than 300 parts in a male human body. These

properties can also be changed according to the system. The implant requires an antenna with small dimensions and it should be long-term biocompatible [Say+09] [Cha+13].

3.3.2 Pulse Shape

Pulse shape is used used to generate bandlimited signals and to reduce the intersymbol interference (ISI) from multipath signal reflections, in order to change the waveform of the transmitted pulses [BM15b].

Since, the transmitted pulses are successively spreading in the time domain, causing a pulse interference in the other, as a result they can interfere with the following or preceding transmitted symbols. This effect is called ISI. When a system has ISI errors, it will be introduced in the decision device at the receiver output. Thus, in the design of the transmitting and receiving filters the goal is to minimize the effects of ISI and therefore deliver the digital data with the smallest error rate possible. In addition to that, the application of a pulse shape filter can be a solution to this problem in order to reduce channel bandwidth and reducing ISI.

The filter itself must do not introduce ISI, consequently it needs to obey to the Nyquist pulse-shaping criterion. So, assuming that the channel is band-limited and has ideal frequency response characteristics ($X(f) = 1$) for transmitted signal $|f| \leq C$. The Nyquist pulse-shaping criterion is settled in the following theorem [Pro01].

Nyquist Theorem

$$h(nT) = \begin{cases} 1, & (n = 0) \\ 0, & (n \neq 0 \end{cases} \tag{3.6}$$

This equation is equivalent to

$$\sum_{\infty}^{m=-\infty} H(f + m/T) = T \tag{3.7}$$

where H(f) is the Fourier transform of h(t).

For using the Nyquist theorem three cases can be discussed. The first case is about a rectangular pulse shaped filter which satifies all the conditions of the Nyquist theorem. Although, the use of a rectangular pulses is generally a poor use of the spectral resources due to the wide spectrum occupancy and poor spectral efficiency. The second case is the sinc shaped filter which satisfies all the conditions and theoretically is considered the best pulse shape filter. However, the sinc-function is infinitely long and it is not practicable as a pulse shape filter [AAS86] [Pro01].

The third and last case is about the raised cosine filter which is practical to implement. It is the most frequently used for pulse-shaping in digital modulation due to its ability to minimize ISI, thus satisfying all the conditions mentioned before.

According to [Pro01] its frequency characteristic is given as:

$$H_{rcc}(f) = \begin{cases} T & \left(0 \leqslant |f| \leqslant \frac{1-\beta}{2T}\right) \\ \frac{T}{2}\left\{1 + cos\left[\frac{\pi T}{\beta}\left(|f| - \frac{1-\beta}{2T}\right)\right]\right\} & \left(\frac{1-\beta}{2T} \leqslant |f| \leqslant \frac{1+\beta}{2T}\right) \\ 0 & \left(|f| > \frac{1+\beta}{2T}\right) \end{cases} \tag{3.8}$$

for $0 \leq \beta \leq 1$ where β is the roll-off factor, T is the symbol rate and $\frac{1}{2T}$ is the excess bandwidth, which is usually expressed as a percentage of the Nyquist frequency. The time domain representation is given by

$$h(t) = \text{sinc}(\pi t/T)\frac{\cos(\pi\beta t/T)}{1 - 4\beta^2 t^2/T^2} \tag{3.9}$$

[Pro01]

The raised cosine filter is a modified version of a sinc function because h(t) is normalized which means that h(0)=1, t, is 1. Figure 3.4 shows the raised cosine spectral characteristics for different values of the roll-off factor, β.

With a raised cosine filter it is possible to design a low-pass filter and high-pass filter for the transmitter and receiver, in order to achieve the desired frequency response, due to its smooth characteristics. Being that the raised cosine filter is the best solution for pulse-shaping to be considering in this case.

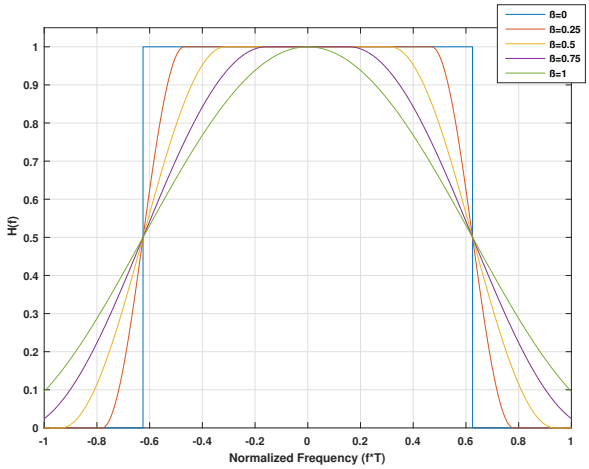

Figure 3.4: Frequency response of raised-cosine filter

The roll-off factor is measured through the excess bandwidth of the filter, which means the bandwidth occupied beyond the Nyquist bandwidth of 1/2T. It modifies the spectrum of signals and the shape of the time-domain properties of digital waveforms.

In order to find a roll-off factor between 0 and 1, which suits better for a $\frac{\pi}{8}$ - D8PSK modulation needs, chapter 4 describes all the simulation procedures.

3.3.3 Additive white Gaussian noise channel

An AWGN is by definition a time-discrete channel with input t and output r=t+a, where, a, is the AWGN. *"Additive"* means added noise to the transmitted signal, *"white"* because the power spectral density is flat at every frequency, so the autocorrelation of the noise in time domain is zero for any non-zero time offset and *"Gaussian"*, because the noise samples have a Gaussian distribution. The model does not account for fading, frequency selectivity, interference, dispersion or nonlinearity. Although, this model is very efficient when simulating background noise or amplifier noise. Then the model can be complemented with impulse noise or other typical noise models. In the following pages the representation of an AWGN channel will be described [AAS86] [YSJ14].

3.4 Modulations

As seen before in the sub-section 3.1, modulation is the process of conveying a message signal. In other words, it transforms a baseband message signal into a pass-band signal. A passband modulation signal can be split in three main categories, analog modulation, digital modulation and spread spectrum.

In this thesis, the focus needs to be centered on the digital modulation, more specifically in PSK and CPM, since those are the modulations which will be studied in the following chapters. A good spectral efficiency can be achieved with these two modulations [Poo15].

A PSK modulation is responsible for changing the phase of sent data, on a radio communication signal in a more efficient manner than frequency shift keying (FSK). In this modulation system, when in the transmitted signal there is a transition from a bit 0 to a bit 1 or vice-versa, a phase reversal will be created. This means the carrier wave has a different phase of 180 degree. This basic form of PSK is called binary phase shift keying (BPSK). When those transitions does not occur, i.e. when the following bits are the same, the data sending continues with the same phase during the transmission [Poo15].

Although, the main problem of a PSK modulation is that the receiver cannot identify where the phase of the transmitted signal is exactly located. To overcome this difficulty a differential method for encoding the data onto the carrier will be applied to the PSK modulations systems [Poo15].

3.4.1 Differential 8-Phase Shift Keying Modulation

A D8PSK modulation is a differential modulation format where the bits for a given symbol are determined by the phase change from the previous symbol. It can be easily implement because there is no need for the demodulator to have a copy of the reference signal to determine the exact phase of the received signal. It does not require the estimation of the carrier phase. One of the biggest advantages of D8PSK modulation

over a PSK modulation is the fact that it avoids the need for a coherent reference signal at the receiver. That means the received signal is compared to the phase of the received signal from the preceding signaling interval [Pro01].

The constellation mapper operates on the binary bit strean $b(n)$, which is the chain of the PLCP preamble, the PLCP header and the PSDU [IEE12]. It takes groups of bits and maps them to specific constellation points. Hence, the differential phase shift keying (DPSK) constellations should be mapped into $\frac{\pi}{8}$ - D8PSK rotation between each symbol, which leads to a physical 16- PSK constellation. The encoded information is carried in the phase transition between symbols. The binary stream $b(n), n = 0, ..., N-1$ should be mapped into a corresponding complex-values sequence $S(k), k = 0, 1, ..., (N/\log_2(M)) - 1$, as equation (3.10) shows [IEE12].

$$S(k) = S(k-1)e^{j\varphi_k}, \quad k = 0, 1, ..., (N/\log_2(M)) - 1 \tag{3.10}$$

Where $S(-1) = e^{j\pi/2}$ is the reference for the first symbol of the preamble, the phase change φ_k is $\frac{\pi}{8}$, and the bit stream for a $\frac{\pi}{8}$ - D8PSK mapping assumes the values $b(3n) = 0$, $b(3n+1) = 0$ and $b(3n+2) = 0$ [IEE12].

Due to this rotation the ideal trajectory constellation between symbols never crosses the zero point as it can be seen in figure 3.5. The constellation mapping represents all the possible symbols used by a transmitted signal data, it also helps to design better communication systems and quickly find a system error. If the trajectory constellation spreads around in circle that means the phase of the signal is being changed. If the trajectory constellation spreads off the circle, either to or away from the origin, then the magnitude of the signal is being changed [Dae15].

Figure 3.5 shows two different trajectories constellations mapping of two different types of modulations. Figure 3.5a shows the trajectory constellation of $\frac{\pi}{8}$ - D8PSK for a encoded 8-PSK modulation. As can be seen the trajectory spreads around the origin in circles, which means the phase is being changed, as expected, since the modulation in matter is D8PSK. On the other hand, figure 3.5b illustrates the trajectory constellation for

a 16-quadrature amplitude modulation (QAM) modulation, which spreads off the circle in direction to the oring. Then the magnitude of the signal is being changed.

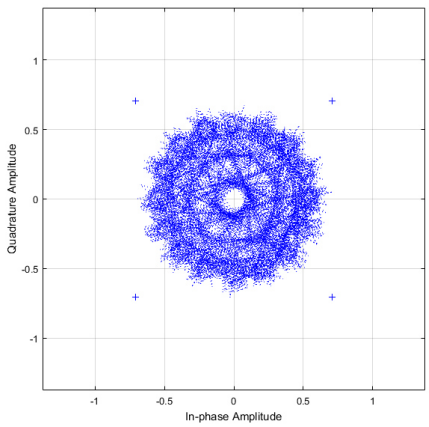

(a) $\frac{\pi}{8}$ - D8PSK modulation trajectories

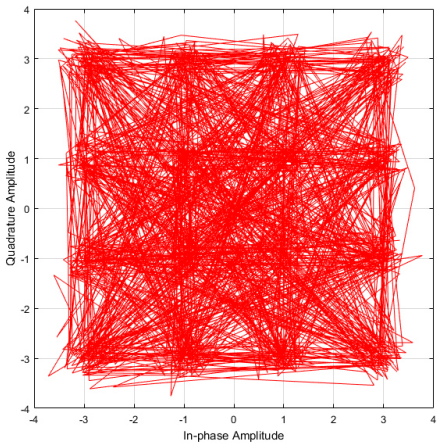

(b) 16QAM trajectories

Figure 3.5: Trajectories comparison

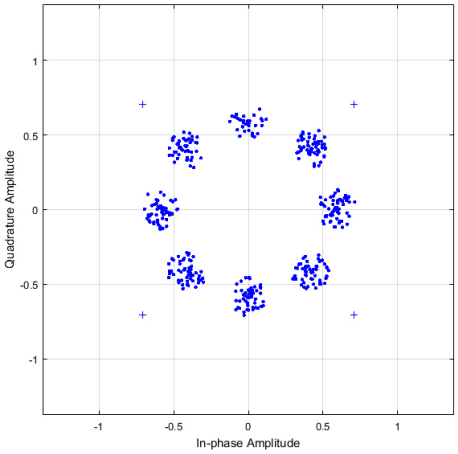

(a) $\frac{\pi}{8}$ - D8PSK constellation diagram

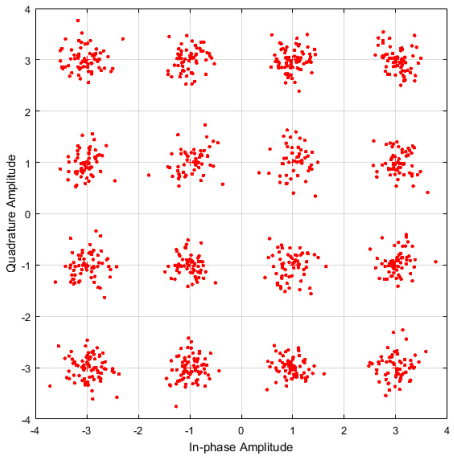

(b) QAM constellation diagram

Figure 3.6: Constellation diagram comparison

Figure 3.6 shows the constellation diagram for the two different types of modulations. The constellation diagram represents a modulated signal by a digital modulation scheme such as QAM or PSK. It represent the possible symbols that may be selected by

the two modulation schemes – $\frac{\pi}{8}$ - D8PSK and 16QAM – as points in the complex plane. Plotting several symbols in a scatter diagram produces the constellation diagram. The points on a constellation diagram are called constellation points. Figure 3.6 shows these constellation points for both modulation schemes. The measured constellation diagrams can be used to recognize the type of interference and distortion in a signal.

The physical layer in 802.15.6 standard utilises a $\frac{\pi}{8}$ - D8PSK as a modulation format, for the highest bit rate of 455.5 kbps as mentioned in sub-section 2.3.1. In chapter 4 this modulation will be explored in detail.

3.4.2 Continuous Phase Modulation

The CPM is a coherent digital phase modulation, which is used as a method for data modulation in wireless modems. It is implemented as a constant envelope waveform, which has a constant carrier power at the transmitter. This implies that the frequency baseband pulse does not contain any impulse for creating a CPM signal. CPM has a high spectral efficiency due to the lack of phase discontinuities which reduces high-frequency spectral content. Although, CPM requires a high implementation complexity for an optimal receiver [AS84].

The transmitted signal of a CPM system is described through the following equation (3.11)

$$x(t,\alpha) = \sqrt{\frac{2E}{T}} cos(2\pi f_0 t + \varphi(t,\alpha) + \varphi_0) \tag{3.11}$$

Where E is the symbol energy, T is the symbol time, f_0 is the carrier frequency and φ_0 is an arbitrary constant phase shift, which can be set to zero without loss generality, in the case of coherent transmission. The CPM transmitted signal always has a constant amplitude [AS81].

The signal $x(t,\alpha)$ has a constant amplitude and the information carrying phase is:

$$\varphi(t,\alpha) = 2\pi h * \sum_i \alpha_i h_i g(t - iT) \tag{3.12}$$

and α_i is an infinetly long sequence of uncorrelated $M-ary$ data symbols for a $\alpha_i = \pm 1, \pm 3, ..., \quad \pm(M-1)$ with equal probability $1/M$. $M-ary$ is an assumed modulation index [AS84]. The variable h represents the modulation index and the amplitude of the baseband pulse *g(t)*, is chosen to give the maximum phase change radians over each symbol interval [AS81]. The modulation index is fixed for all symbols, that means when $h_i = h$ for all i. When the modulation index varies from one symbol to another, the CPM scheme is called multi-h. Consequently the h_i is made to vary in a cyclic manner through a set of indices, otherwise, h is assumed to be fix [AAS86].

CPM schemes are denoted by their phase response function or by its derivative $g(t)$, the frequency response function. Therefore, CPM can be divided into full response signaling and partial response signaling system. A full response signaling occurs when in the transmitted signal the instantaneous frequency is just affected per each data symbol in one symbol interval and its phase is continuous along the time. A partial response signaling occurs when the instantaneous phase of the transmitted signal is modulated by the data symbols and the phase is continuous on time-domain. Although, one single data symbol affects this phase more than one symbol interval [AS81].

In practice, a system is considered a full response signaling, for a pulse length equal or less than one and is considered a partial response signaling for a pulse length greater than one. That brings us to the pulse shape of a CPM. The most commonly CPM pulse shapes used are rectangular frequency pulse length L (LREC), raised cosine, pulse length L (LRC) and Gaussian minimum-shift keying (GMSK). The prefix "L'' denotes the length of the response. Equations (3.13), (3.14) and (3.15) show the most common pulse shapes with their frequency responses.

LREC

$$g(t) = \begin{cases} \frac{1}{2LT} & (0 \leq 1 \leq LT) \\ 0 & (otherwise) \end{cases} \tag{3.13}$$

LRC

$$g(t) = \begin{cases} \frac{1}{2LT}\left(1 - cos(\frac{2\pi t}{LT})\right) & (0 \leq 1 \leq LT) \\ 0 & (otherwise)) \end{cases} \tag{3.14}$$

GMSK

$$g(t) = Q[2\pi B\left(t - \frac{T}{2}\right)/(ln2)^2]$$

$$Q(t) = \int_t^\infty \frac{1}{\sqrt{2\pi}} e^{-x^2/2} dt \tag{3.15}$$

In the first function of equation (3.15) the parameter B is arbitrary and it is set to obtain the desired distance or spectral properties. The L parameter in equation (3.13) and equation (3.14) is a positive integer. The most important schemes for a full response signaling are the 1 raised cosine (RC) and the 1 rectangular frequency pulse (REC) [AAS86].

As mentioned before, CPM is a constant amplitude modulation scheme which can be a generalization of continuous phase frequency shift keying (CPFSK) or minimum shift keying (MSK). The lack of phase discontinuities reduces high-frequency spectral content [Pro01]. CPFSK signals have a continuous phase and they can be modulated onto a sinusoidal carrier wave, encoding the information present in the data to variations in the carriers instantaneous frequency. This modulation is frequently used in signals that are transmitted over a bandlimited channel due to its continuous phase characteristics. It is considered as an alternative name for the 1 REC family [AAS86]. MSK can be seen as a case of binary CPFSK with a modulation index equal to $h = \frac{1}{2}$, or as a special case of offset quadrature phase shift keying (OQPSK) with rectangular pulse with T duration [Pro01] [AAS86].

The GMSK pulse is a infinite time duration and therefore, time-truncated in time domain implementations. GMSK with a bandwidth of $B = 0.3$, is used in the european digital cellular communication sytem, called GSM [AAS86].

3.4.3 General Overview Channel Model for Both Modulations

Figure 3.7 represents the general overview of a channel model for D8PSK and CPM modulation. At the transmitter the input symbols b_k generate random bits for a PSDU of 255 octets, as mentioned in the IEEE Std. 802.15.6. Then, these bits will be decoded through a BCH code, mapped in compliance with the modulation method (DPSK modulator or CPM modulator) and the pulse shape with a raised-cosine filter, $p(t)$. After that, the transmit filter will be amplified using a nonlinear power amplifier ($g(A)$) which will be the Rapp model amplifier as mentioned before.

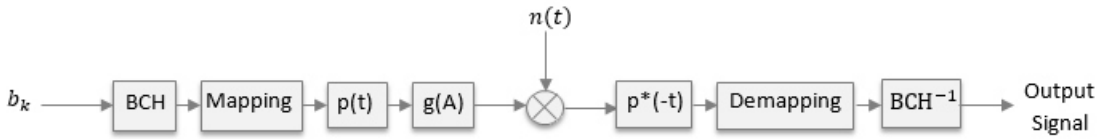

Figure 3.7: General overview of a modulation channel model, p(t) represents the pulse shape (RRC) and g(A) the power amplifier

An AWGN will be added to the noise, at the receiver. The received signal will be demodulated, demapped and decoded in order to obtain the output signal. Afterwords the received data will be compared with the transmitted data through a BER/Frame error rate (FER) versus SNR plot.

After nonlinear amplification, the transmitted signal passed through the AWGN channel where Gaussian noise with two-sided PSD $n_0/2$ is added to it. Physically, the additive noise process may ascend from electronic components and amplifiers at the receiver of the communication system or from interference encountered in transmission. Since the noise is primarily introduce by an amplifier at the receiver, it can be characterized as thermal noise. Therefore, the mathematical result for the channel model is called additive white Gaussian noise channel.

Thermal noise is characterized statistically as a white Gaussian noise process and extends over a very wide spectrum. The noise power is proportional to the bandwidth,

which follows this equation

$$v^2 = 4 \cdot K \cdot T \int_{f1}^{f2} R \ \ dF \tag{3.16}$$

Where v represents the integrated root mean square (RMS) voltage between the frequencies range, R is the resistive component of impedance, T represents the temperatures in Kelvin (K = C + 273.16) and the frequencies, f_1 and f_2, the lower an upper limits of the required bandwidth [Pro01] [Poo15].

The thermal noise equation can be simplified, when the resistive component of the impedance remains constant over the required bandwidth.

$$v = \sqrt{4 \cdot K \cdot T \cdot B \cdot R} \tag{3.17}$$

In order to determine the thermal noise in terms of power level, is necessary to consider the noise resistor as an ideal resistor connected in series with a noise voltage source and connected to a matched load. This is given by equation (3.18) [Poo15].

$$N = \frac{v^2}{4R} <=> N = \frac{\sqrt{4KTBR}}{4R} <=> N = KTB \tag{3.18}$$

In view of calculate the total thermal noise characteristics at the receiver. The noise figure of the receiving device needs to be added to the equation (3.18).

Equation (3.19) is used to estimate the expected total thermal noise at the receiver. The parameter K is a Boltzman constant, so $k = 1.3807 * 10^{-23} \quad (J/k)$, T represents the ambient temperature in Kelvin, given by 300 Kelvin and B is the bandwidth in Hertz, which will assume the value of 300 kHz (given by the IEEEStd. 802.15.6 page 190). N_F is the noise figure and assumes the value of 20dB.

After all the calculations, the power thermal noise is given by equation (3.20) in decibel.

$$N = KTB <=> N = 1.2426 \cdot 10^{-15} \ (W/Hz) \tag{3.19}$$

$$N_{total,dB} = 20 \cdot log_{10}(KTB) + N_{F,dB} <=> N_{total,dB} = 100 \ (dBm) \tag{3.20}$$

3.5 Summary

In this chapter can be concluded that a PA is used to reduce the losses between the transmitter and the receiver. In order to isolate the effects in the SSPA a pulse shape with RRC filter is used in the channel model. A SSPA is an amplifier which uses transsistors to provide useful amplification at higher frequencies. In the simulation the Rapp model will be use as a nonlinear model of a PA.

From the second section of this chapter can be retain that a channel model is used to convey information signals from the transmitter side to the receiver side. The path loss describes the signal attenuation between the transmitter and the receiver antenna. The pulse shape obey to the Nyquist criterion and uses a RRC filter.

From the end on this chapter can be conclude that both modulations signals are a current interest for terrestrial mobile data communication due to the achievement of a good spectral efficiency.

4 MATLAB Simulation and Results

The theoretical background approached in the previous chapters were the pillar to build a time-domain simulation model for MATLAB.

The goal of this simulation consists in the comparison of two modulation schemes, $\frac{\pi}{8}$ - D8PSK and CPM, in terms of power efficiency and linearity requirements.

A Monte Carlo method was used in the computer simulation. The transmitted data was generated through random symbols for all the considered modulations. The bits were encoded using a BCH code. The PSDU use a BCH(63,51) encoder and it is simulated with a MATLAB toolbox function, ***comm.BCHEncoder(N,K)***. Where N, represents the codeword length and it assumes the value 63, while K represents the message length assuming the value 51, as explained in subsection 2.4.1.

The waveforms were generated by passing a modulator and a raised cosine (RC) pulse shape filter, as mentioned in the previous chapter. The Rapp model was used as a nonlinear PA. After the nonlinear amplification, the signal passed through the AWGN channel where a Gaussian noise is added to the channel model. The received signal is filtered.

The decision on the data is made after sampling the output of the filtered signal. The received bit sequence is compared with the transmitted data sequence, in order to calculate the BER/FER versus the SNR.

In the following sections a description of the three blocks represented in figure 4.1 will be shown, as well as an explanation of the parameters values used along this simulation.

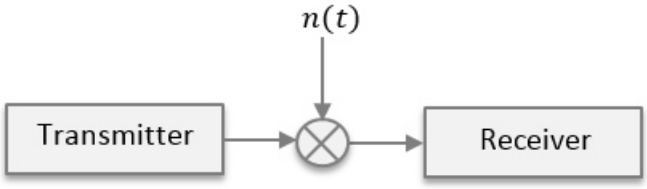

Figure 4.1: Channel model

Some of the MATLAB functions mentioned in this chapter can be found in the appendix of this dissertation and all of the MATLAB functions can be found on the attached disc in the MATLAB simulation folder.

This chapter is divided in three sections, the first is related to the transmitter model, the second to the simulation channel and the third to the receiver model. Since $\frac{\pi}{8}$-D8PSK and CPM use different modulators, a different explanation of both modulation schemes can be found in each aforementioned section.

4.1 Evalutation of Transmit Characteristics

The parameters used in both modulation schemes along this simulation from the transmitter blocks will be approached.

$\frac{\pi}{8}$ - D8PSK modulation will be analysed in a first step, followed by the CPM. In this second modulation scheme the choice of the values to use as input parameters are related. That means the choice of a modulation index (h) interferes with the choice of a M-ary value (M), as well as with the choice of the pulse shape (L). Therefore, all those values will be chosen with a reasonable explanation based on scientific grounds and already conducted studies.

As it already has been discussed in chapter 3, the transmitter model consists of four steps: a BCH encoder, a constellation mapping, a pulse-shape andamplifier, as visualized in figure 3.7.

In order to investigate the self and adjacent-channel interference in both modulation schemes, an auto-correlation function and a PSD is used. The auto-correlation is the cross correlation of a signal with itself, in order to find some repetition at some different points in time. The comparison between the transmitted signal before and after the amplifier was plotted in order to detect the autocorrelation (figure 4.2). The figure shows that the transmitter signal before the amplifier matches perfectly with the signal after the amplifier. The autocorrelation value is approximately 3000.

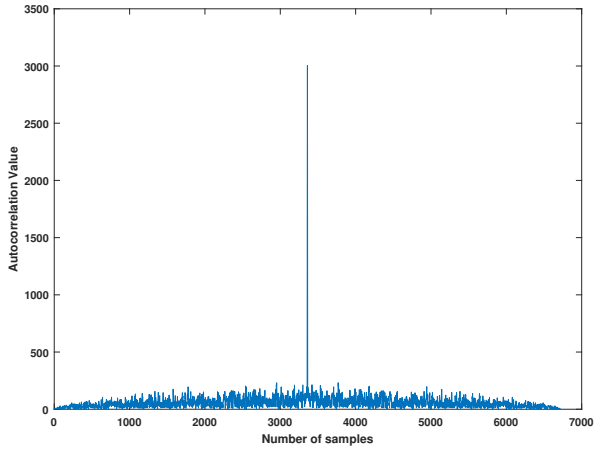

Figure 4.2: D8PSK - Autocorrelation of a transmitted signal before and after the amplifier with 1 Watt

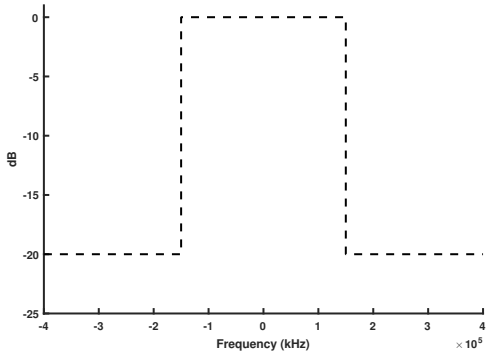

Figure 4.3: Transmit spectral mask for all frequency bands

The transmit PSD mask is used along all the simulation process, which should be

less than -20 dBr. The dB is relative to the maximum spectral density of the signal. For MICS band frequencies (402-405MHz) the channel bandwidth is 300kHz and is a function of the frequency band of operation as illustrated in figure 4.3.

4.1.1 Differential 8-Phase Shift Keying

This subsection explains a baseband simulation model for $\frac{\pi}{8}$ - D8PSK modulation. From the transmitter point of view in a D8PSK modulator, every three input data bits are mapped to one complex valued D8PSK symbol. It uses an 8-ary as a modulation order. Each symbol with a $\frac{\pi}{8}$ rotation phase between each symbol is BCH encoded prior to mapping them to the $\frac{\pi}{8}$ - D8PSK constellation. In $\frac{\pi}{8}$ - D8PSK there are eight possible symbols that can be transmitted. In this simulation, a $\frac{\pi}{8}$ phase represents each of the eight symbols, as shown in figure 3.6a of subsection 3.3.1. After that, a RRC pulse shape filter is added to the channel model. The RRC filter produces a frequency response with unity gain at low frequencies and ends at higher frequencies. Mathematically the RRC filter is defined as equation (4.1), described in subsection 3.2.2.. The roll off factor, represented by β, determines the sharpness of the frequency response. The frequency response of the RRC filter is shown in figure 4.4. If we look at the β=0.5, the excess bandwith is 50 percent and when β=1, the excess bandwidth is 100 percent.

In this simulation, the roll off factor assumes a value of 0.6, (β=0.6). This value is the closest to the spectral mask with an excess bandwidth of 60 percent.

The channel model uses a Rapp model for the PA, as mentioned before is chapter 3. The Rapp model has an adjustable knee sharpness for SSPA using AM/AM conversion. It is able to provide any desired sharpness parameter and it follows equation (4.1).

$$g(A) = \frac{vA}{[1 + (\frac{vA}{A_0})^{2p}]^{\frac{1}{2p}}} \tag{4.1}$$

Where $g(A)$ is the output amplitude, A is the input amplitude, v the small signal gain, A_0 the output limit amplitude and p represents the sharpness parameter. The sharpness

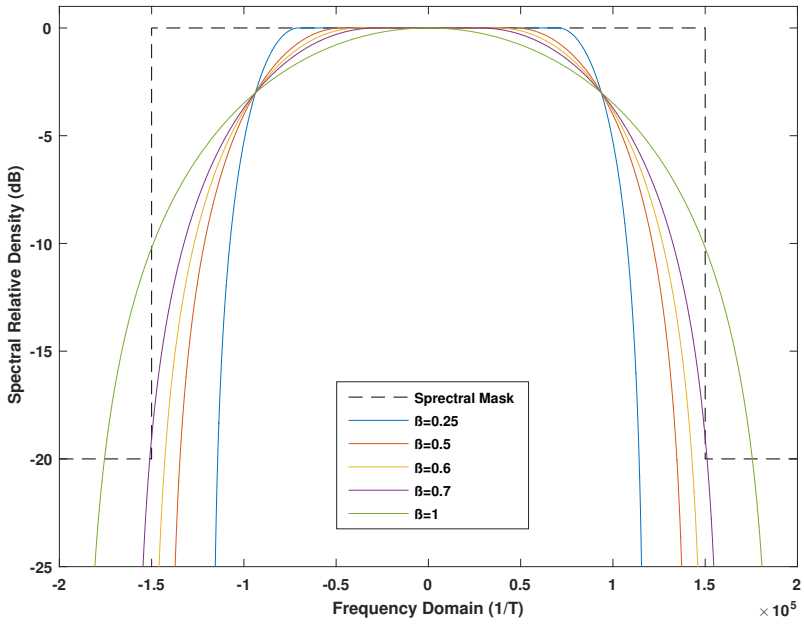

Figure 4.4: Frequency response of a root raised cosine filter with various roll-off factors

paramenter controls the smoothness of the transition from the linear region to the limiting region. In the MATLAB simulation, the variables v and A_0 assumed a constant value ($v = 1$, $A_0 = 1$) and A is represented by the input signal. A range from 1 to 5 values of sharpness parameters (p) were taken into consideration. The resulting amplitude transfer function for some different values of p are plotted in figure 4.5 for unity limit level and small signal gain. With the parameter p = 3 the measured characteristic of 1-Watt SSPA is well approximated [Can12].

A comparison of a non-ideal amplifier and an ideal amplifier is taken into consideration along this simulation. Some literature, e.g. [Can12], defends that in the region above $p = 2.5$ the most real amplifiers reside. Following that, $p = 3$ is the sharpness parameter value which will be used and it represents a non-ideal amplifier.

An ideal amplifier should be obtained when a real amplifier is ideally linearized. The AM/AM is ideally linear up to the limiting output amplitude, where it remains constant. This is limited by the following equation (4.2) for an ideal amplifier, p = ∞ [Rap91].

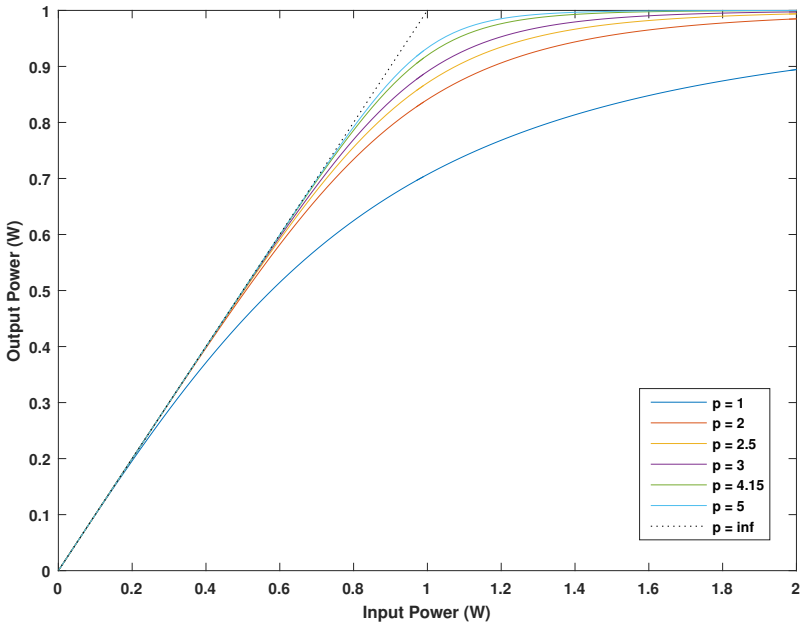

Figure 4.5: Rapp's envelope model characteristics for p=0,1,2,2.5,3,4.15,5

This function is used in the MATLAB simulator to define the ideal amplifier.

$$\lim_{p->\infty} g(A) = \begin{cases} v * A_0 & , A > A_0 \\ v * A & , |A| \leq A_0 \\ -v * A_0 & , A < -A_0 \end{cases} \tag{4.2}$$

According to the previous information, from the transmitter side, the values to take into consideration are: a BCH(63,51), a RRC filter pulse shape β=0.6, a power range between 0.5 Watt and 1 Watt, a sharpness parameter equal to $p = 3$ and $p = \infty$ for the PA block of the channel model. After that, the D8PSK symbols are transmitted over an AWGN channel that adds Gaussian noise to the transmitted symbol.

4.1.2 Continuous Phase Modulation

As seen before a CPM is characterized by a continuous phase and it is a nonlinear modulation technique with memory. A transmitted CPM signal always has a constant amplitude.

Following the same line of thinking of the D8PSK modulation channel model. After generating the random bits, each symbol is BCH encoded and then the bits are mapped. A MATLAB toolbox function is used, ***comm.ConstellationDiagram ('SamplesPerSymbol',M)***, where M represents the modulation index. A CPM is described by various trajectories from one phase state to another. For a constant amplitude CPM signal, the various trajactories form a circle as figure 4.6 shows. This phase trajectory represents the trajectory constellation for a CPM with a modulation index of $h = 1/4$ and a modulation order (M-ary) of $M = 4$. The phase trajectory is represented in the figure by a continuous circle. Note that the length of the phase trajectory increases with an increase in h. When the modulation index increases, also the signal bandwidth increases.

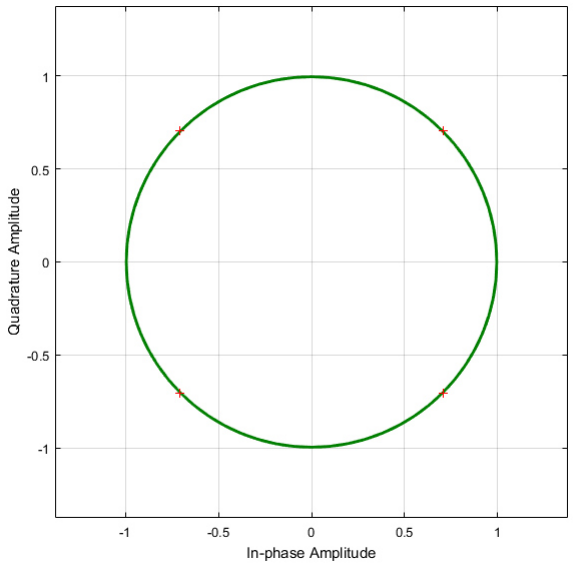

Figure 4.6: Contellation mapping of a continuous phase modulation

CPM can be divided into full response and partial response, which brings to the

first decision. Which type of signal response should be used in this simulation? As it is known, the type of signal response is related with the pulse length. If the pulse length is $L \leq 1$ the signal has a full response. If the pulse length is $L > 1$ the signal has a partial response. The following figures represent the plots which helped in the choice of the length of the pulse shape and the type of pulse shape.

As mentioned in chapter 3, there are several common CPM pulse shapes. In order to select the pulse shape to be used in this simulation, the equations of those CPM pulse shapes are plotted for two values of modulation order, $M = 4$ and $M = 8$, and two different values of modulation index, $h = 0.25$ and $h = 0.5$. On the horizontal axis the frequency is plotted and on the vertical axis the input power to the amplifier is plotted. The sellection of these parameters will be explained in the following pages.

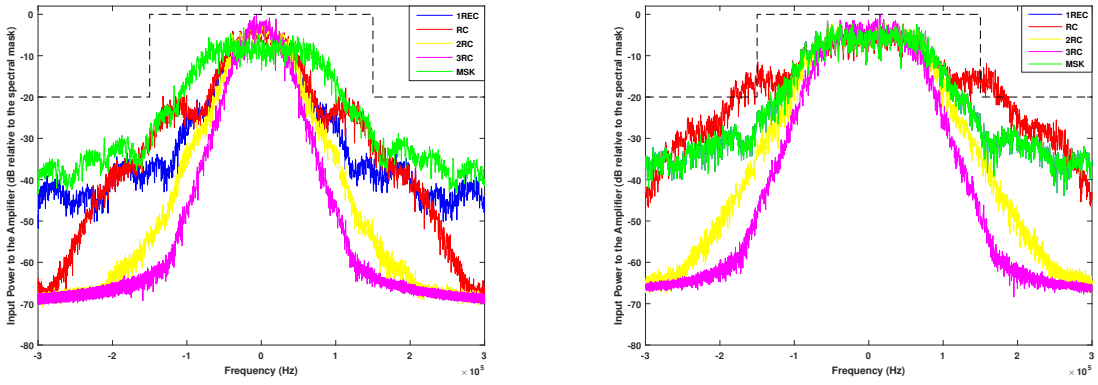

(a) PSD with h=0.25

(b) PSD with h=0.5

Figure 4.7: Power Spectrum Density of M=4 for 1REC, 1RC, 2RC, 3RC and MSK pulse shape

Figure 4.7 illustrates the power spectrum density for $M = 4$ CPM and figure 4.8 shows the PSD for a $M = 8$ CPM. Both plots have represented differential partial response LRC, REC and MSK pulses when $h = 0.25$ – figure 4.7a, for $M = 4$ and figure 4.8a for $M = 8$ – and $h = 0.5$ – figure 4.7a for $M = 4$ and figure 4.8b for $M = 8$.

1REC and RC represent the full response signaling. The other pulse shapes represent the partial response signaling. For comparison, it is evident how the smoothing

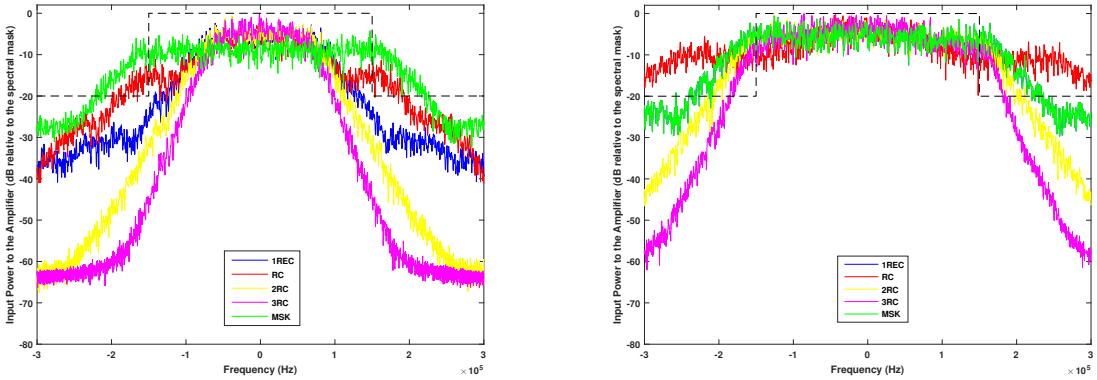

(a) PSD with h=0.25

(b) PSD with h=0.5

Figure 4.8: Power Spectrum Density of M=8 for 1REC, 1RC, 2RC, 3RC and MSK pulse shape

of the phase trajectories with 2RC and 3RC considerably improves the spectral properties of the constant amplitude scheme, for both different values of modulation index and order. Consequently, a RC filter is selected as an ideal frequency pulse shape scheme to be used in this simulation.

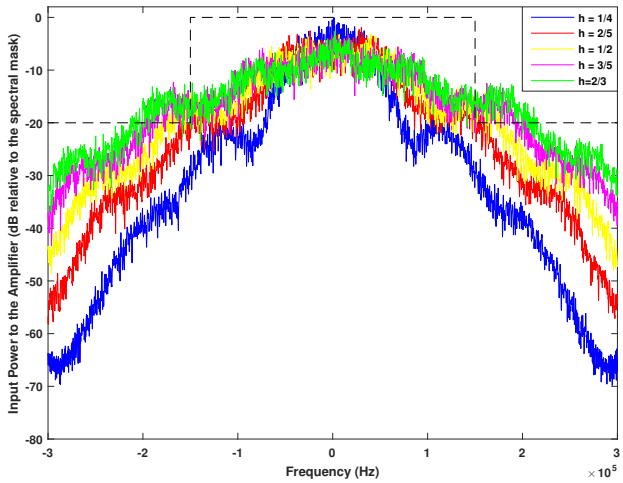

Figure 4.9: Power spectrum density for M=4 CPM with RC and different modulation indices

In order to decide which is the most reasonable value of modulation index to be used in this simulation, the plot of different modulation indices for different pulse length RC filter will be observed.

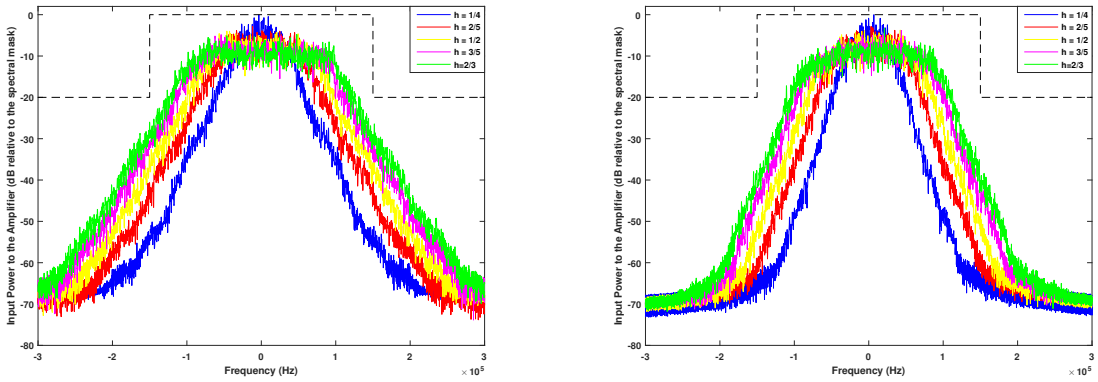

(a) PSD with 2 Raised Cosine Pulse Shape (b) PSD with 3 Raised Cosine Pulse Shape

Figure 4.10: Power spectrum density for M=4 CPM with different modulation indices and pulse shapes

Figures 4.9 and 4.10 illustrate the input power to the amplifier for a $M = 4$ CPM with three different length of pulse shape. From the comparison of these figures it is obvious to conclude that the modulation index 0.25 ($h = 1/4$) is inside the spectral mask for all values of pulse length L in a RC filter. Some literature, e.g. [AS81], defends that a 3RC partial response signaling of CPM should be used due to its simple implementation. Therefore, the full response signaling is excluded from that simulation. Thus, the CPM modulator in this simulation uses a $L = 3$ and the frequency pulse shape is RC.

In consideration of CPM being a class of digital modulations with constant amplitude, the memory is introduced in the signals by means of the continuous phase. Being an advantage for both power spectral properties and detection properties. For partial response schemes further memory is introduced by means of controlled intersymbol interference. From the data presented above can be concluded that power efficient digital modulation schemes can be obtained using a 3RC, $M = 4$ and $h = 0.25$ (Note that a $h = 0.25$ also can be use in a full response signal). Although, that brings one disadvan-

tage: the increased complexity. The complexity can be obtained through the increasing of M and L. However, following the study of [AS81] about the Viterbi detector, which grows with L and M according to the equation (4.3).

$$S = pM^{L-1} = p2^{b(L-1)} \tag{4.3}$$

Exponentially with the pulse length L and the number of bits b per level ($M = 2^b$). From that it is obvious to conclude that both M and L should be chosen as small as possible. Thus, if two schemes are comparable in performance, such as 3RC, $M = 8$ and 3RC, $M = 4$ in figure 4.8 and figure 4.7, the $M = 4$ is considerably simpler to implement.

The following values have been used as parameters of the CPM modulator: a modulation index of $h = 1/4$, the modulation order assumed the value $M = 4$ and a 3RC was considered as the requency pulse shape. As in the $\frac{\pi}{8}$ - D8PSK modulation, a Rapp model non-linear amplifier will be used in CPM.

4.2 Simulation of Channel Model

The transmitted channel model has a BCH(63,51) block, a RRC pulse shape filter with a roll off factor of $\beta = 0.6$, a non-linear amplifier with different levels of nonlinearity (power range between, $InputPower = 0.5 \quad (Watt)$ and $InputPower = 1 \quad (Watt)$ and two values of sharpness parameter, $p = 3$ and $p = \infty$. These blocks are equally used in both modulations schemes. The modulation order use in $\frac{\pi}{8}$ - D8PSK is $M = 8$.

Figure 4.11 shows the power spectral density of a transmitted signal before and after the amplifier, for an $InputPower = 0.5$ Watt (figure 4.11a) and an $InputPower = 1$ Watt (figure 4.11b)for a p=3 of a $\frac{\pi}{8}$ - D8PSK. As it can be seen the amplifier influence is not significant for an $InputPower = 0.5$ Watt as shown in figure 4.11a. If the input power is increased to one, the difference from the transmitter signal before the amplifier and the transmitted signal after the amplifier is relevant, as shown in figure 4.11b. Thus, it can be concluded that a high input power value influences in the transmitted signal.

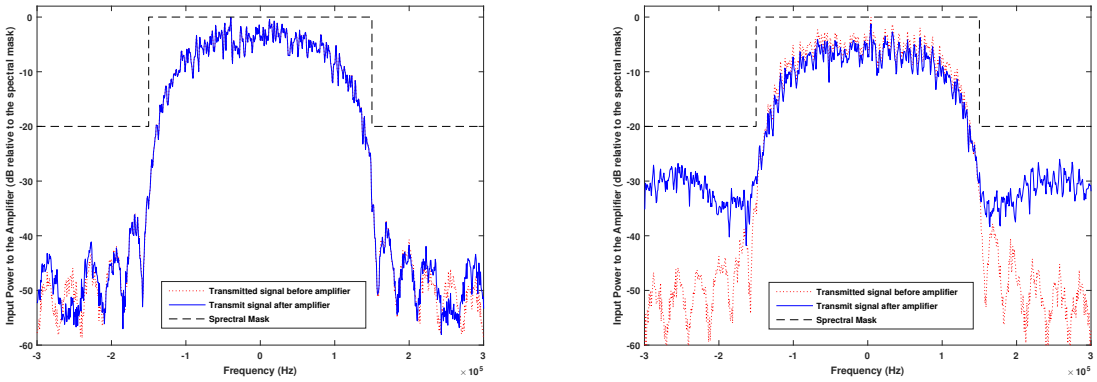

(a) Input Power = 0.5 Watt (b) Input Power = 1 Watt

Figure 4.11: D8PSK - Power spectral density of a transmitted signal before and after the amplifier

In order to obtain the highest power value for each type of amplifier to be used in the transmitted signal and in order to guarantee that it is inside the spectral mask, a simulation of PSD for an ideal amplifier and nonideal amplifier were plotted, as figure 4.12 represents. Therefore, for an ideal amplifier ($p = \infty$) the maximum power is $InputPower = 0.69 \quad Watt$ and for a nonideal amplifier ($p = 3$) the maximum power is $InputPower = 0.89 \quad Watt$.

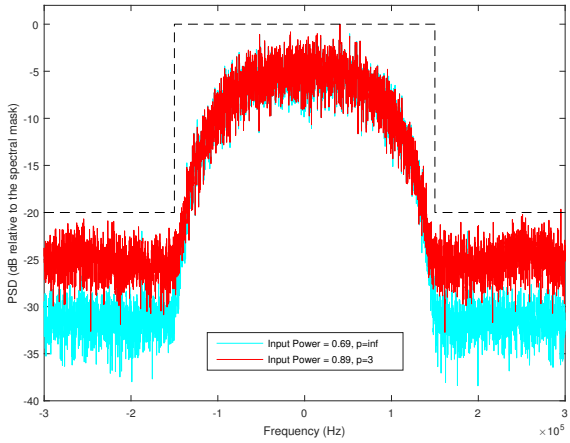

Figure 4.12: D8PSK - Power spectral density of a transmitted signal after the amplifier

A PSD for a CPM can be observed in figure 4.13 which represents the minimum input power value $InputPower = 0.5Watt$ (figure 4.13a) and the maximum input power value $InputPower = 1Watt$ (figure 4.13b) for CPM. From these figures can be observed that for the minimum input power value ($InputPower = 0.5Watt$) the transmitted signal is influenced by the input power value. But for higher input power values these influence decreases. Therefore, it can be concluded that for a CPM the lower input power value influences in the transmitted signal.

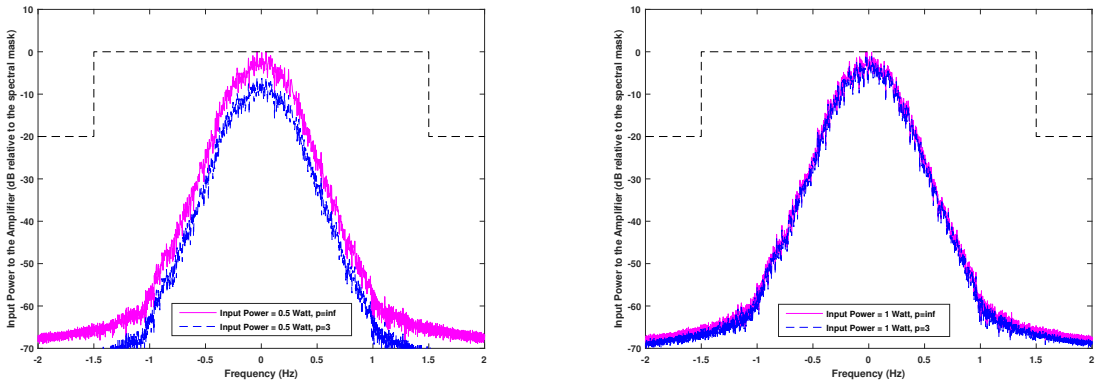

(a) Input Power = 0.5 Watt

(b) Input Power = 1 Watt

Figure 4.13: CPM - Power spectral density of a transmitted signal before and after the amplifier

4.3 Evaluation of Receiver Characteristics

The transmitted $\frac{\pi}{8}$ - D8PSK and CPM baseband signals can be expressed in complex form as

$$s(t) = \sqrt{\frac{2E}{T}} \sum_{i=\infty}^{\infty} I(t - iT) e_{j\varphi(t,\alpha)} \tag{4.4}$$

Where E denotes the average received signal energy per symbol, T represents the symbol interval and α the waveform shaping pulse [BH99]. In order to filtered the $\frac{\pi}{8}$ - D8PSK

modulation, $I(t)$ is the impulse response of a RRC filter and it satisfies the Nyquist criterion for zero ISI. The $\varphi(t, \alpha)$ represent the information-carrying phase, which for this modulation is $\frac{\pi}{8}$. The signal $s(t)$ is transmitted over an AWGN channel. The receiver observes the signal $r(t) = s(t) + n(t)$ where $s(t)$ is the transmitted signal and $n(t)$ represents the AWGN noise.

The receiver structure for $\frac{\pi}{8}$ - D8PSK modulation and CPM is described bellow.

4.3.1 Differential 8-Phase Shift Keying Modulations

At the receiver the detection process is performed by finding one of the eight constellation symbols that has the smallest Euclidean distance with the received symbol. Some may prefer to use a sector based detection approach in which the received signal constellation is divided into sectors.

For D8PSK, the entire constellation can be equally divided into eight sectors, with each angle of the sector corresponding to one of the eight constellation symbols. The detection process can be performed by using the angle of sectors. Instead of this approach, this simulation is based on minimum Euclidean Distance. The detector computes the Euclidean distance of each received symbol against all possible ideal symbols. Then it pin points an ideal symbol which gives the minimum Euclidean distance. It is computed using the following equation (4.5).

$$D = \sqrt{[(y_r - s_r)]^2 + (y_i - s_i)]^2} \tag{4.5}$$

Where y represents the received signal (with noise), s represents the points on ideal constellation and the subscripts r and i are for their real and imaginary part respectively.

The detector calculates the Euclidean distance of a received symbol against all possible symbols in the constellation and picks a symbol from the ideal constellation that gives the minimum Euclidean Distance.

Finally, the demodulated symbols are converted back to binary bits and the BER is calculated.

4.3.2 Continuous Phase Modulation

It is assumed that the frequency response is a 3RC, the modulation order is $M = 4$ and the modulation index is $h = 1/4$. An optimal receiver for a CPM signal consists of a correlator followed by a maximum likelihood sequence detector that searches the paths through the state trellis for the minimum Euclidean distance path. The Viterbi algorithm is an efficient method for performing this search [AS81]. A trellis is used to choose among possible extensions of those paths. Following the study made in [AS81] can be concluded that the minimum Euclidean distance is sufficient for the characterization performance in terms of symbol error probability. Even when the upper bound is loose the minimum distance appears to be accurate. The squared Euclidian distance can be writen as equation (4.6)

$$D^2(\alpha_{K,N}, \alpha_{l,N}) = \int_0^{NT} [s(t, \alpha_{K,N}) - s(t, \alpha_{l,N})]\, \partial t \tag{4.6}$$

When a calculation of the minimum Euclidean distance is performed, the first pair of data symbols must be deifferent by definition, and hence, the phase trajectories are always different over this symbol interval.

4.4 Simulation Results of D8PSK and CPM

The transmitted symbols are detected as reliably as possible at the receiver end, given a specific SNR, for most digital communications systems. The symbol error probability should be minimized because it is a common used criterion among in communication engineering.

By definition BER is a parameter which gives an excellent indication of the performance of a radio data link. As one of the main parameters of interest in any data link is the number of errors which occur, therefore BER is a key parameter. The knowledge about the BER also enables other features of the link such as the input power and bandwidth.

BER testing is a powerful method for end to end testing of digital transmission systems and a BER test can provide a measurable and useful indication of the performance of the system which can be directly related to its operational performance. If the BER rises too high then the system performance will noticeably degrade. If it stays within certain limits, the system will operate satisfactorily.

In most cases, the performance of a code under a particular decoding algorithm is characterized by the BER or the FER curve plotted as a function of the SNR.

The BER performance was simulated by adding noise between 0 to 20 dB to the transmitted signal. This noisy signal is added to the input receiver signal. As mentioned in subsection 3.3.3, at the transmitter the input symbols generate random bits for a PSDU of 255 octets for a packet error rate of less than or equal to 10% in AWGN channel. This number of octets is considered the frame size of the transmitter signal, in order to determine the FER performance. In the end, the receiver demodulates the signal producing a sequence of recovered bits. The FER is the ration of frames in error to the total number of frames.

Finally, the received bits are compared with the transmitted bits and plot of the errors through BER versus SNR.

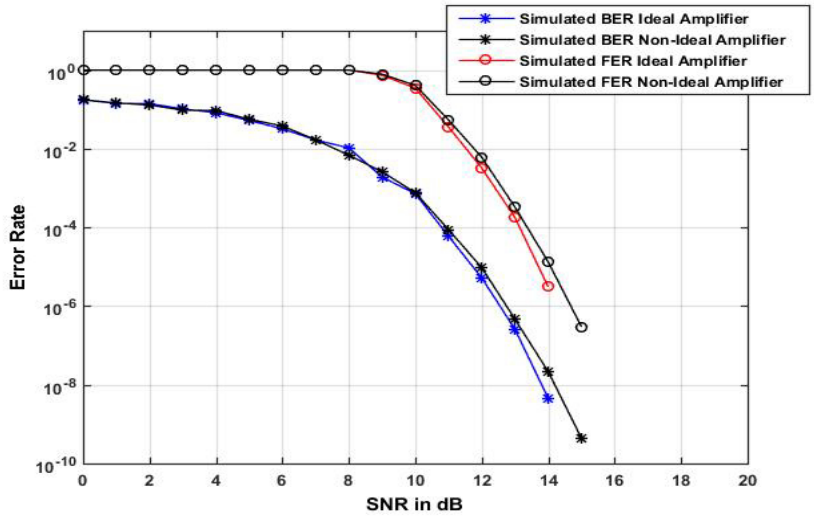

Figure 4.14: BER vs SNR for D8PSK different power values

From figure 4.11b the maximum input power values for an ideal and a non-ideal amplifier are determined. Thus for an ideal amplifier the maximum input power value used is $InputPower = 0.69$ Watt and for a non-ideal amplifier the input power value used is $InputPower = 0.89$ Watt, as mentioned before.

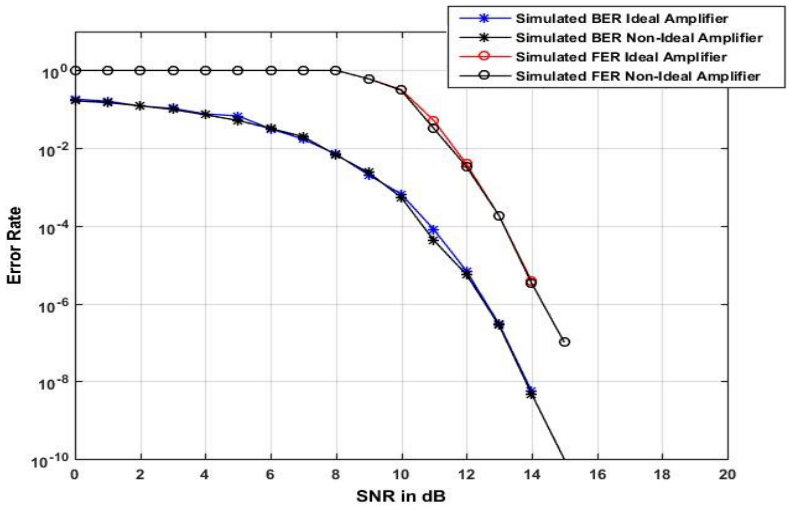

Figure 4.15: BER vs SNR for D8PSK same power values

Therefore figure 4.14 illustrates the BER/FER curve plotted as a function of the SNR of the $\frac{\pi}{8}$ - D8PSK modulation with the maximum input power values for the different types of amplifiers. This curve consists of two distinct regions, BER and FER. At small SNR, the FER probability is uniform until a SNR = 9dB. Afterwords the FER curve decreases rapidly for higher values of SNR like a waterfall. On the other hand, the BER slope decreases slowly for small SNR and after a SNR = 7dB it decreases rapidly.

Figure 4.15 illustrates the BER/FER curve plotted as a function of the SNR of the $\frac{\pi}{8}$ - D8PSK modulation with the minimum input power value ($InputPower = 0.5 \quad Watt$) for the different types of amplifiers. BER and FER curves have a similar behavior as in figure 4.14. Though in this case the BER/FER curve for an ideal and non-ideal amplifier has the same shape. From that can be concluded that the amplifier has no influence in the channel model of a $\frac{\pi}{8}$ - D8PSK modulation. That means the amplifier does not influence or change the signal behavior which means that the signal has a constant amplitude. The

$\frac{\pi}{8}$ - D8PSK modulation is characterized for conveying data by changing the phase of the carrier wave.

Note that for an ideal amplifier the error probability of bits and frame assumes a zero value for SNR equal to 15dB in both plots. The simulation of BER/FER versus SNR for a $\frac{\pi}{8}$ - D8PSK modulation ran for three days.

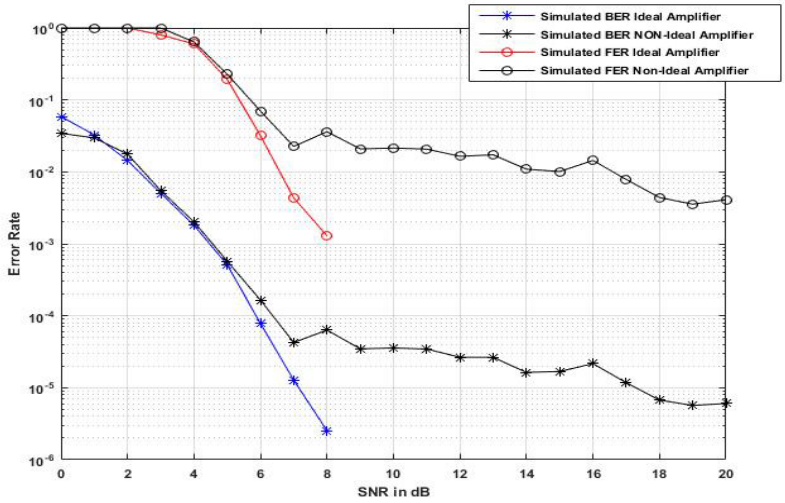

Figure 4.16: BER vs SNR for CPM the minimum power value (Input power = 0.5 Watt)

Also for the CPM modulation the BER/FER curves are plotted as a function of the SNR as shown in the coming plots. Figure 4.16 represents the BER/FER versus SNR curves of CPM modulation with the minimum input power value ($InputPower = 0.5 \quad Watt$) for the two different types of amplifiers used in this simulation. Figure 4.17 illustrates the BER/FER versus SNR curves of CPM modulation with the maximum input power. This plot considers the same maximum input power used in a $\frac{\pi}{8}$ - D8PSK modulation and the maximum input power of a CPM modulation – $InputPower = 1 \quad Watt$.

At small SNR values, the BER and FER probability curves decrease rapidly with SNR, making them look like a waterfall. In the BER/FER curves of a non-ideal amplifier the decrease slows down at a SNR=7dB due to the back-to-back penalty system. Even when the signal does not have any noise the signal has errors. The back-to-back penalty in this sytem is BER=10^{-5} and FER=10^{-3}. Naturally the system never goes below than

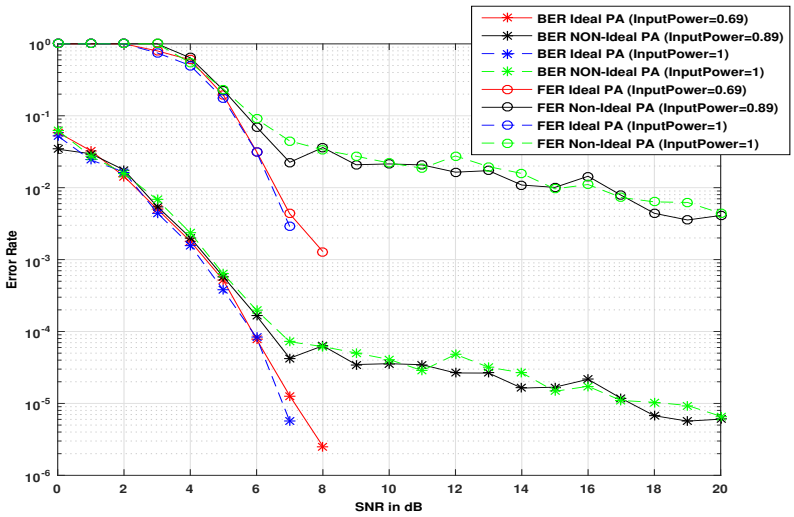

Figure 4.17: BER vs SNR for CPM different maximum input power values (0.69Watt, 0.89Watt and 1 Watt)

this BER/FER curve values. That just happens for a non-ideal amplifier because the back-to-back penalty in this amplifier is bigger than in an ideal amplifier. That means the demodulation process in a non-ideal amplifier is not efficient as it is for an ideal amplifier.

From the results obtained in the previous figures can be observed that at an error rate of BER=10^{-5} the difference in SNR between the two modulations is less than 1dB.

It is obvious to conclude that the BER decreases as the SNR increases, thus the system operates satisfactorily for both modulation schemes. Note that the BER and FER have been measured by comparing the transmitted signal with the received signal and computing the error count over the total number of bits or frames (in the case of FER). For any given modulation, the BER and FER are normally expressed in terms of SNR.

5 System Performance and Final Results

The error rate performance of $\frac{\pi}{8}$ - D8PSK and CPM with this data-aided linear and non-linear receiver was evaluated by means of computed simulation for different values of input power.

As the FER curve for lower values of SNR does not have a relevant error performance, it is excluded from the next plots. So just the BER performance curve is illustrated in the following figures for both modulations. This simulation ran for four days and the results were obtained for a SNR =10 dB.

The average bit error probabilities of the proposed receiver were evaluated by computer simulations for $\frac{\pi}{8}$ - D8PSK and CPM signal through a AWGN channel.

Figure 5.1 illustrates the minimum input power value used ($InputPower$ = 0.5 Watt) and figure 5.2 represents the maximum input power values of $\frac{\pi}{8}$- D8PSK for an ideal amplifier ($InputPower_{Max,D8PSK}$ = 0.69 Watt) and for a non-ideal amplifier ($InputPower_{Max,D8PSK}$ = $0.89Watt$), as well as for a CPM ($InputPower_{Max,CPM}$ = 1 Watt), for the two types of amplifiers analyzed in this thesis.

The simulation results indicate that the proposed receiver of a CPM modulation performes better than a $\frac{\pi}{8}$ - D8PSK modulation. From the graph shown in figure 5.1, it can be observed that at an error rate of BER=10^{-3} the difference in SNR between $\frac{\pi}{8}$- D8PSK and CPM is approximately 5 dB. If the simulation would have run more time, probably

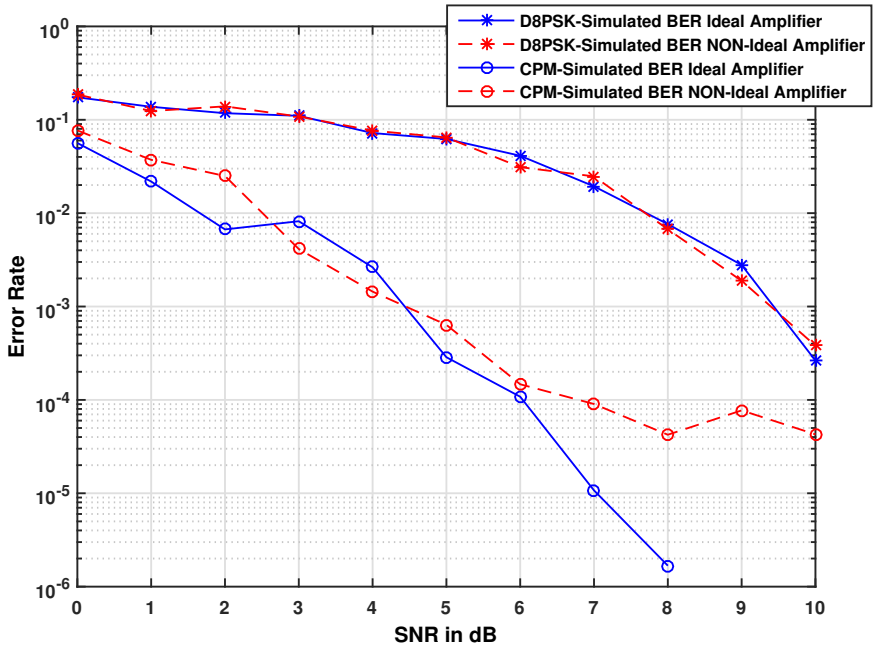

Figure 5.1: Minimum input power value (0.5 Watt)

the difference in SNR of an ideal and non-ideal amplifier for both modulations will be less than 1 dB.

The performance of an ideal amplifier for a $\frac{\pi}{8}$ - D8PSK is similar to a non-ideal amplifier performance – as concluded before in subsection 4.4. Due to the fact that the amplifier in $\frac{\pi}{8}$ - D8PSK does not influence the signal behavior, it only impacts the phase signal.

On the other hand, the type of amplifier has a different behavior on a signal with CPM, as shown in both figures for the minimum and maximum input power values. The performance degradation for an ideal amplifier occurs at 8 dB in SNR for BER=10^{-6}. However, for a non-ideal amplifier the performance degradation is about 10 dB in SNR for BER=10^{-4}. This draws the conclusion that an ideal amplifier of a CPM reaches a better performance.

Due to these results it is obvious to conclude that an ideal amplifier has an overall better performance compared to a non-ideal amplifier.

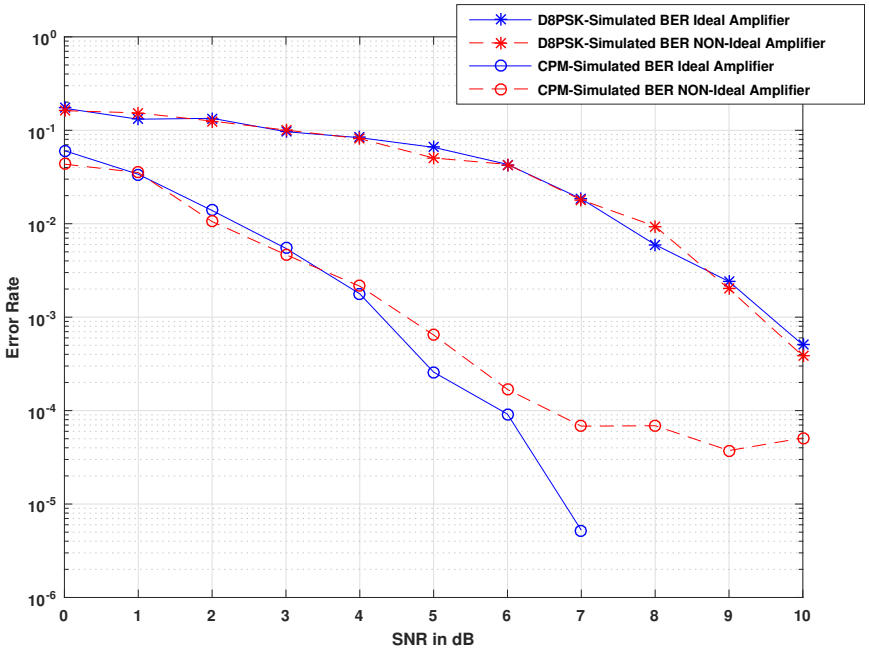

Figure 5.2: Maximum input power values, 0.69 Watt for an ideal amplifier and 0.89 Watt for a non-ideal amplifier in a D8PSK modulation and 1 Watt for both amplifiers in a CPM.

5.1 Power Efficiency

In order to determine which modulation has a better power performance with the different types of amplifiers, the power efficiency of this simulation is considered here. By definition power efficiency is defined as the ratio of the output power divided by the input power.

The SNR is fixed to 7 dB because as shown in figure 5.1 and figure 5.2, the ideal amplifier of a CPM detects errors until a BER=10^{-6} for a SNR=7 dB. After that value the error performance is BER=0. The input power range is between 0.5 Watt and 1 Watt. Figure 5.3 illustrates that performance.

After observing the performance plot, it can be concluded that CPM has a better performance than a $\frac{\pi}{8}$ - D8PSK modulation. The input power has a constant performance in

a CPM modulation for an ideal amplifier, once BER=10^{-5} between the defined input power range. For a $\frac{\pi}{8}$ - D8PSK modulation the value of BER oscillates. For a non-ideal amplifier the BER=10^{-2} and for an ideal amplifier the BER value oscillated from BER=10^{-3} to BER=10^{-2} in the same power range. This means that the CPM modulation guarantees a better accuracy of the signal than a $\frac{\pi}{8}$ - D8PSK for both types of amplifiers.

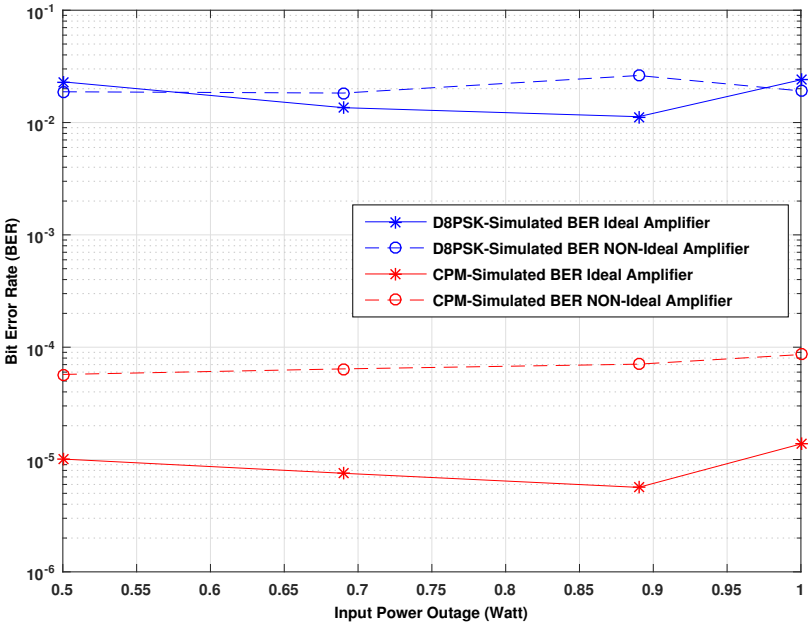

Figure 5.3: Power efficiency of D8PSK and CPM modulations for different input power values (0.5 Watt, 0.69 Watt, 0.89 Watt and 1 Watt)

5.2 Frame Error Rate over a Distance in Human-Body Channel

In order to analyze for which distances these two modulations can work in a real life implementation, a link budget for the MICS band transmission of an implant to implant application is analyzed. As mentioned in the beginning, implanted sensors for the medical surveillance of patients are approached in this thesis. These implants can be located in deep tissue or near surface (e.g cardiac pacemaker). Thus, in this section, the measurements of distances for each location of the implant are described.

First of all the maximum transmitting power must be prescribed. In [WW12] is mentioned that the MICS band allows a maximum transmitting power of 25 μW or -16 dBm. Although, a 20 mW or 13 dBm can also be an acceptable value for transmitting power, from the point of view of biological safety. In this study both values will be used.

A link budget is the accounting of all of the gains and losses from the transmitter, through the transmission medium T_x to the receiver in a communication system. The link budget can be determined using equation 5.1.

$$Recived \quad Power(dBm) \quad = \quad T_x(dBm) \quad - \quad P_L(dB) \quad - \quad N(dBm) \tag{5.1}$$

The noise power characteristics at the receiver are the first to be determined. Assuming that the only noise source at the receiver is AWGN, which usually it is typically thermal. Following the equation 3.17 – subsection 3.3.3 – the thermal noise power is $N_{total,dBm} = 100\ dBm$.

The second parameter to be determined is the path loss (in dB) which follows the equation 3.3 – subsection 3.2.1. The parameters for an implant to implant communication scenario in deep tissues and near surface can be found in table 5.1. S is the random scatter around the mean and represents deviation in dB caused by different materials and antenna gain in different directions. Considering a simple case of an environment where there are no objects or obstacles, a free space path loss can be estimated. Thus, S is an excluded

value from equation (5.2).

$$PL(d_{dB}) = PL(d_0) + 10 \cdot \eta \cdot log_{10}\left(\frac{d}{d_0}\right), d \geq d_0 \tag{5.2}$$

Where $PL(d_0)$ assumes the value 35.04 dB and $\eta = 6.26$ for a deep tissue implant and $PL(d_0)$ assumes the value 40.94 dB and $\eta = 4.99$ for a near surface implant; d_0 is the reference distance and assumes the value 50 mm for both implant locations. These values are referenced by [Say+09].

Following the results obtained in the previous chapter about the plot of BER versus SNR, it can be concluded that for a $\frac{\pi}{8}$ - D8PSK modulation the system works until a SNR=13 dB and for a CPM until SNR=9 dB. For a $\frac{\pi}{8}$ - D8PSK modulation the system works for SNR values greater than 13 dB because a PSDU length of 255 octets is used in the power of interfering signal which is raised until a 10% packet error rate (PER) [IEE12].

Table 5.1: Parameters for the statistical path loss model of implant to implant channel [Say+09]

Implant to Implant	$PL(d_0)$(dB)	η
Deep Tissue	35.04	6.26
Near Surface	40.94	4.99

In order to calculate at which distances this system can work, the equation 5.1 is used as shown in equation 5.3.

$$\begin{aligned} SNR_{dB} &= 10 \cdot log_{10}(T_x - PL(d_{dB}) - N_T) \\ <=> 10^{\left(\frac{SNR_{dB}}{10}\right)} &= T_x - PL(d_{dB}) + N_T \end{aligned} \tag{5.3}$$

Replacing $PL(d_{dB})$ for equation (5.2) the SNR_{dB} is given by equation (5.4).

$$\begin{aligned} & 10^{\left(\frac{SNR_{dB}}{10}\right)} - T_x - N_T + PL(d_0) = -10 \cdot \eta \cdot log_{10}\left(\frac{d}{d_0}\right) \\ <=> & \frac{10^{\left(\frac{SNR_{dB}}{10}\right)} - T_x - N_T + PL(d_0)}{-10 \cdot \eta} = log_{10}\left(\frac{d}{d_0}\right) \\ <=> & 10^{\left(\frac{(10^{\left(\frac{SNR_{dB}}{10}\right)} - T_x - N_T + PL(d_0))}{-10 \cdot \eta}\right)} = \frac{d}{d_0} \\ <=> & d = 10^{\left(\frac{(10^{\left(\frac{SNR_{dB}}{10}\right)} - T_x - N_T + PL(d_0))}{-10 \cdot \eta}\right)} \cdot d_0 \end{aligned} \tag{5.4}$$

Making all the replacements for the values mentioned before, table 5.2 and table 5.3 show the distances for each location of the implant. It also shows the distances for a maximum transmitting power, -16 dBm and for a biological safety power, 13 dBm.

Table 5.2: Distance values for both modulations for a deep tissue implant

Deep Tissue	Distance for $T_x = -16(dBm)$	Distance for $T_x = 13(dBm)$
D8PSK (SNR = 13 dB)	14.53 (cm)	42.23 (cm)
CPM (SNR = 9 dB)	22.60 (cm)	65.68 (cm)

Table 5.3: Distance values for both modulations for a near surface implant

Near Surface	Distance for $T_x = -16(dBm)$	Distance for $T_x = 13(dBm)$
D8PSK (SNR = 13 dB)	14.52 (cm)	55.36 (cm)
CPM (SNR = 9 dB)	25.28 (cm)	96.35 (cm)

It is obvious to say that the better distances results are obtained for a safe biological power, 13 dBm with both implant implementations. For near surface implant-to-implant the distance results are even smaller than deep tissue implants. So, from these measurements it can be concluded that with a CPM system can be obtained higher distances than in a $\frac{\pi}{8}$ - D8PSK modulation. This happens due to the continuous phase characteristics of CPM. Although for a $\frac{\pi}{8}$ - D8PSK modulation the system can also reach higher distances with the increase ofSNR values.

6 Conclusions

This thesis approaches the use of implant sensors for medical surveillance of patients. However, the goal of this thesis aims to try to assist in the discovering how these sensors are supposed to be implanted for a long time in terms of energy efficiency.

For that two different modulations were analyzed: a $\frac{\pi}{8}$ - D8PSK modulation and a CPM. The first is characterized by its phase shift keying which avoids the need for a coherent reference signal at the receiver. The second modulation is characterized by its continuous phase, where the carrier phase is modulated in a continuous manner.

In the first part of this thesis a research about the channel modelling for BAN concepts and the non-linear effects in power amplifiers were investigated, in order to understand the basic techniques which are used along this thesis. Since the implant sensors are extremely small it was important to consider the implementation cost given by the IEEE 802.15.6 Standard.

In order to test all of this theoretical background, a MATLAB simulation was used. Consequently, a channel model was built followed by all the standardization values and definitions. It was divided in three parts: the first related to the transmitter signal, the second to the simulation channel and the third to the received signal.

In the first model lies the central piece of the simulation part: the transmitter signal. The input symbols generated random bits for a PSDU of 255 octets. Then those bits were encoded through a BCH code, followed by a D8PSK modulator or CPM modulator, depending on the modulation type in question, a RRC filter pulse shape and finished with

a nonlinear amplifier, called Rapp model. A AWGN was added to the noise at the receiver and the signal was demodulated, demapped and decoded in order to obain the plot of the BER vs SNR.

After the analysis of all the simulation results obtained during the research, it can be concluded that in a $\frac{\pi}{8}$ - D8PSK modulation an ideal and non-ideal amplifier show a similar behavior. This means that the amplifier does not influence or change the signal dealings. This brings us to the conclusion that the signal has a similiar behavior to a constant amplitude. This is not the case for CPM, where the ideal an non-ideal amplifiers have different behaviors. Although for a non-ideal amplifier it was found that the demodulation process is not efficient as it is for an ideal amplifier using the same modulation.

The BER performance is clearly better in a continuous phase modulation. It can achieve an error performance of BER= 10^{-6} for SNR = 7dB. Although that points to a for CPM to compared to $\frac{\pi}{8}$ - D8PSK modulation in the matter of finding up to which distances the implant can communicate with an external device. From the estimated distance values $\frac{\pi}{8}$ - D8PSK modulation delivers better results.

The simulation results indicate that the continuous phase modulation is a good option to use in implanted sensors due to its simple implementation and the use of simple power amplifiers.

6.1 Recommendations and Future Research

Future work is needed to simulate for which distances the implanted transmitter sensor should be located to reach the receiver based on the calculations made. In order to make the system work for further distances. The impact of the energetic consumption of a transmitter within the body and its workability is also considered as a future field of study. A deep study on how this implant sensor can be implemented from the transmission side and how it could be used in real life applications is also strongly recommended.

Perhaps, this system can be studied for optical communication instead of radio frequency communication. For the continuous phase modulation (CPM) other modulation orders and modulation indices can be analyzed as well as the usage of other pulse shapes. Further viterbi and trellis can be calculated and simulated for a CPM. In order to have a better performance of the two modulations the transmitter and the receiver should be optimized.

Bibliography

[AAS86] J. B. Anderson, T. Aulin, and C.-E. Sundberg. *Digital Phase Modulation*. Applications of communications theory. New York: Plenum-Pr, 1986, pp. 45–53 & 181–209.

[AS81] T. Aulin and C.-E. Sundberg. "Continuous Phase Modulation–Part I: Full Response Signaling and Part II: Partial Response Signaling". In: *Communications, IEEE Transactions on* 29.3 (Mar. 1981), pp. 196–225.

[AS84] T. Aulin and C.-E. Sundberg. "CPM – an efficient constant amplitude modulation scheme". In: *International Journal of Satellite Communications* 2.3 (1984), pp. 161–186. URL: http://dx.doi.org/10.1002/sat.4600020304.

[BH99] L. Bin and P. Ho. "Data-aided linear prediction receiver for coherent DPSK and CPM transmitted over Rayleigh flat-fading channels". In: *Vehicular Technology, IEEE Transactions on* 48.4 (July 1999), pp. 1229–1236.

[BM15a] J. N. Bringuier and R. Mittra. *Electromagnetic Wave Propagation in Body Area Networks Using the Finite-Difference-Time-Domain Method*. Dec. 3, 2015. URL: http://www.ncbi.nlm.nih.gov/pmc/articles/PMC3435949/.

[BM15b] J. N. Bringuier and R. Mittra. "Pulse-Shape Filtering in Communications Systems". In: (Dec. 8, 2015). URL: http://www.ni.com/white-paper/3876/en/.

[Can12] A. Cann. "Improved Nonlinearity Model With Variable Knee Sharpness". In: *Aerospace and Electronic Systems, IEEE Transactions on* 48.4 (Oct. 2012), pp. 3637–3646.

[Cha+13] R. Chavez-Santiago, K. Sayrafian-Pour, A. Khaleghi, et al. “Propagation models for IEEE 802.15.6 standardization of implant communication in body area networks”. In: *Communications Magazine, IEEE* 51.8 (Aug. 2013), pp. 80–87.

[Cha81] W. M. Chardack. “Recollections–1958-1961”. In: *Pacing and Clinical Electrophysiology* 4.5 (1981), pp. 592–596.

[Cro15] G. Crouch. *Testing BAN WBAN Networks and IEEE 802.15.6, National Instruments*. May 7, 2015. URL: http://www.ni.com/tutorial/14285/en/#toc2%201/7.

[Dae15] I. Daemon. Dec. 13, 2015. URL: http://www.inetdaemon.com/tutorials/basic_concepts/communication/signals/constellation.shtml.

[FBB08] I. Frigyes, J. Bito, and P. Bakki. “Advances in Mobile and Wireless Communications: Views of the 16th IST Mobile and Wireless Communication Summit”. In: Lecture Notes in Electrical Engineering (2008). URL: https://books.google.de/books?id=C3jrJ28%5C_-1YC.

[GR94] R. Garud and M. A. Rappa. “A socio-cognitive model of technology evolution: The case of cochlear implants”. In: *Organization Science* 5.3 (1994), pp. 344–362.

[Gri+87] B. P. Griffith, R. L. Hardesty, R. L. Kormos, et al. “Temporary Use of the Jarvik-7 Total Artificial Heart before Transplantation”. In: *New England Journal of Medicine* 316.3 (1987). PMID: 3540665, pp. 130–134. eprint: http://dx.doi.org/10.1056/NEJM198701153160303. URL: http://dx.doi.org/10.1056/NEJM198701153160303.

[Han15] Y. Han. *Decoding BCH or RS Codes*. Nov. 26, 2015. URL: http://web.ntpu.edu.tw/~yshan/BCH_decoding.pdf.

[IEE12] IEEE. “IEEE Standard for Local and metropolitan area networks - Part 15.6: Wireless Body Area Networks”. In: *IEEE Std 802.15.6-2012* (Feb. 2012), pp. 172–196.

[IEE15] IEEE. *802.11 PHY Layers - Chapter8*. Nov. 24, 2015. URL: http://media.techtarget.com/searchMobileComputing/downloads/CWAP_ch8.pdf.

[int15] C. research international. Dec. 3, 2015. URL: http://www.cygres.com/OcnPageE/Glosry/SpecE.html.

[Iye+11] S. S. Iyengar, N. Parameshwaran, V. V. Phoha, et al. *Fundamentals of Sensor Network Programming: Applications and Technology*. John Wiley & Sons, 2011.

[KN12] A. Kiourti and K. Nikita. "A Review of Implantable Patch Antennas for Biomedical Telemetry: Challenges and Solutions [Wireless Corner]". In: *Antennas and Propagation Magazine, IEEE* 54.3 (June 2012), pp. 210–228.

[Lee+09] C. Lee, J. Kim, H. S. Lee, et al. "Physical layer designs for WBAN systems in IEEE 802.15.6 proposals". In: (Sept. 2009), pp. 841–844.

[Lia+99] C.-P. Liang, J.-H. Jong, W. Stark, et al. "Nonlinear amplifier effects in communications systems". In: *Microwave Theory and Techniques, IEEE Transactions on* 47.8 (Aug. 1999), pp. 1461–1466.

[Moo15] T. Moon. *Lecture 7 Decoding BCH codes*. Nov. 26, 2015. URL: http://ocw.usu.edu/Electrical_and_Computer_Engineering/Error_Control_Coding/lecture7.pdf.

[MS15] S. Manjula and D. Selvathi. *Optimal Design of Low Power CMOS POwer Amplifier Using Particle Swarm Optimization Technique*. Vol. 82. 4. Springer, 2015, pp. 2275–2289.

[Neb02] F. Nebeker. "50 Years of the IEEE Engineering in Medicine and Biology Society and the Emergence of a New Discipline". In: *IEEE 50 EMBS* (2002), pp. 1–47.

[Poo15] I. Poole. Dec. 13, 2015. URL: http://www.radio-electronics.com/info/rf-technology-design/pm-phase-modulation/what-is-psk-phase-shift-keying-tutorial.php.

[Pos09] S. Poslad. In: (2009). URL: http://dx.doi.org/10.1002/9780470779446.fmatter.

[Pro01] J. G. Proakis. *Digital Communications*. English. McGraw-Hill Series in Electrical and Computer Engineering, 2001, pp. 185–199 & 272–300 & 556–561.

[Rap91] C. Rapp. "Effects of HPA-nonlinearity on a 4-DPSK/OFDM-signal for a digital sound broadcasting signal". In: (Oct. 1991), pp. 179–184.

[Rit+14] R. Ritter, J. Handwerker, T. Liu, et al. "Telemetry for Implantable Medical Devices: Part 1 - Media Properties and Standards". In: *Solid-State Circuits Magazine, IEEE* 6.2 (Spring 2014), pp. 47–51.

[RP14] H. S. Ruiz and R. B. Perez. *Linear CMOS RF Power Amplifiers*. Springer, 2014.

[Sav+05] H. Savci, A. Sula, Z. Wang, et al. "MICS transceivers: regulatory standards and applications [medical implant communications service]". In: (Apr. 2005), pp. 179–182.

[Say+09] K. Sayrafian-Pour, W.-B. Yang, J. Hagedorn, et al. "A statistical path loss model for medical implant communication channels". In: (Sept. 2009), pp. 2995–2999.

[Sch+70] J. C. Schuder, H. Stoeckle, J. H. Gold, et al. "Experimental ventricular defibrillation with an automatic and completely implanted system". In: 16.1 (1970), pp. 207–212.

[SDC09] S. Sen, S. Devarakond, and A. Chatterjee. "Low cost AM/AM and AM/PM distortion measurement using distortion-to-amplitude transformations". In: (Nov. 2009), pp. 1–10.

[Sem15] Z. Semiconductor. July 3, 2015. URL: `http://stf.ucsd.edu/presentations/2007/2007-08%20STF%20-%20Zarlink%20ULP%20transceivers.pdf`.

[Wal15] H. Wallace. *Error Detection and Correction Using the BCH Code*. Nov. 26, 2015. URL: `http://www.aqdi.com/bch.pdf`.

[Wil15] L. P. Williams. *Hermann von Helmholtz*. Sept. 28, 2015. URL: `http://www.britannica.com/biography/Hermann-von-Helmholtz`.

[WW12] J. Wang and Q. Wang. *Body Area Communications*. John Wiley & Sons (Asia) Pte Ltd, 2012. URL: http://dx.doi.org/10.1002/9781118188491.fmatter.

[YSJ14] S. K. Yakhlef, N. A. A. Shashoa, and M. Jalboub. "Nonlinearity Amplifier Effects on QPSK Technique". In: (Mar. 2014). URL: http://www.academia.edu/8326817/Nonlinearity_Amplifier_Effects_on_QPSK_Technique.

[Zhe15] W. Zhehu. *Chapter 5 BCH Codes*. Nov. 25, 2015. URL: http://cwww.ee.nctu.edu.tw/course/channel_coding/chap5.pdf.